The Astrophysical Journal Supplement Series, 173:104–136, 2007 November
© 2007. The American Astronomical Society. All rights reserved. Printed in U.S.A.

THE STELLAR POPULATION OF THE CHAMAELEON I STAR-FORMING REGION[1]

K. L. Luhman
Department of Astronomy and Astrophysics, The Pennsylvania State University, University Park, PA 16802; kluhman@astro.psu.edu
Received 2007 March 6; accepted 2007 May 24

ABSTRACT

I present a new census of the stellar population in the Chamaeleon I star-forming region. Using optical and near-IR photometry and follow-up spectroscopy, I have discovered 50 new members of Chamaeleon I, expanding the census of known members to 226 objects. Fourteen of these new members have spectral types later than M6, which doubles the number of known members that are likely to be substellar. I have estimated extinctions, luminosities, and effective temperatures for the known members, used these data to construct an H-R diagram for the cluster, and inferred individual masses and ages with the theoretical evolutionary models of Baraffe and Chabrier. The distribution of isochronal ages indicates that star formation began 3–4 and 5–6 Myr ago in the southern and northern subclusters, respectively, and has continued to the present time at a declining rate. The IMF in Chamaeleon I reaches a maximum at a mass of 0.1–0.15 $M_{\odot}$ and thus closely resembles the IMFs in IC 348 and the Orion Nebula Cluster. In logarithmic units where the Salpeter slope is 1.35, the IMF is roughly flat in the substellar regime and shows no indication of reaching a minimum down to a completeness limit of 0.01 $M_{\odot}$. The low-mass stars are more widely distributed than members at other masses in the northern subcluster, but this is not the case in the southern subcluster. Meanwhile, the brown dwarfs have the same spatial distribution as the stars out to a radius of 3° (8.5 pc) from the center of Chamaeleon I.

Subject headings: infrared: stars — stars: evolution — stars: formation — stars: low-mass, brown dwarfs — stars: luminosity function, mass function — stars: pre–main-sequence

1. INTRODUCTION

The characteristics of the distributions of masses, ages, and positions in a newborn stellar population are determined by the process of star formation. As a result, measurements of these distributions in star-forming regions are potentially valuable for testing models of the birth of stars and brown dwarfs. For instance, the properties of the stellar initial mass function (IMF; Meyer et al. 2000) can constrain the relative importance of turbulent fragmentation (Padoan & Nordlund 2002), gravitational fragmentation (Larson 1985), dynamical interactions (Bonnell et al. 2003), and accretion and outflows (Adams & Fatuzzo 1996) in regulating the final masses of stars. Models of the star formation rates of molecular clouds (e.g., constant, accelerating, bursts) can be tested against the distributions of ages and positions of members of young clusters (Feigelson 1996; Palla & Galli 1997; Hartmann 2001). The spatial distributions also provide insight into cloud fragmentation, binary formation, cluster dynamics, and the origin of brown dwarfs (Larson 1995; Hillenbrand & Hartmann 1998; Hartmann 2002; Luhman 2006). To obtain measurements of this kind, one must identify the members of star-forming regions and estimate their masses and ages. Only a few young stellar populations have been characterized in detail, such as the Orion Nebula Cluster (Hillenbrand 1997), Taurus (Kenyon & Hartmann 1995), and IC 348 in Perseus (Luhman et al. 2003b).

The Chamaeleon I star-forming region is amenable to a thorough census of its stellar population for several reasons. It is among the nearest star-forming regions ($d = 160$–170 pc, Whittet et al. 1997; Wichmann et al. 1998; Bertout et al. 1999), exhibits less extinction than many young clusters ($A_V \lesssim 5$), is compact enough that a large fraction of the region can be surveyed to great depth in a reasonable amount of time, and is sufficiently rich for a statistically significant analysis of its stellar population. In addition, because Chamaeleon I is relatively isolated from other star-forming regions, confusion with other young populations is minimal. Previous surveys have already identified more than 150 young stars and brown dwarfs in Chamaeleon I through photometric variability, Hα emission, X-ray emission, mid-infrared (IR) excess emission, and optical and near-IR color-magnitude diagrams (Comerón et al. 2004; Luhman 2004a, 2007 and references therein). However, in the census of known members produced by these surveys, the completeness as a function of mass and position is unknown (Luhman 2004a). In this paper, I present a set of magnitude-limited surveys for members of Chamaeleon I that have well-defined completeness limits (§ 2). I then use the new census of Chamaeleon I to measure the star formation history (§ 3), IMF (§ 4), and spatial distribution of its stellar population (§ 5).

2. NEW MEMBERS OF CHAMAELEON I

2.1. *Selection of Candidate Members*

I have used optical and near-IR broadband photometry from several sources to perform four surveys for new members of Chamaeleon I. The fields covered by these surveys are indicated in the maps of the cluster in Figure 1. The first survey (hereafter named IK1) is shallow ($I \sim 18$) and covers most of the cloud complex, concentrating on the central $1.5° \times 0.35°$ area where most of the known members reside. The second survey (RI) also focuses on this central field but with greater depth ($I \sim 21$). These two surveys are designed to produce an IMF measurement that has good number statistics and completeness to reasonably low

[1] Based on observations performed with the Magellan Telescopes at Las Campanas Observatory, Cerro Tololo Inter-American Observatory (CTIO), Gemini Observatory, and the NASA/ESA *Hubble Space Telescope* (*HST*). CTIO is operated by the Association of Universities for Research in Astronomy (AURA) under a contract with the National Science Foundation (NSF). Gemini Observatory is operated by AURA under a cooperative agreement with the NSF on behalf of the Gemini partnership: the NSF (US), the Particle Physics and Astronomy Research Council (UK), the National Research Council (Canada), CONICYT (Chile), the Australian Research Council (Australia), CNPq (Brazil), and CONICET (Argentina). The *HST* observations are associated with proposal ID 10138 and were obtained at the Space Telescope Science Institute, which is operated by AURA under NASA contract NAS 5-26555.

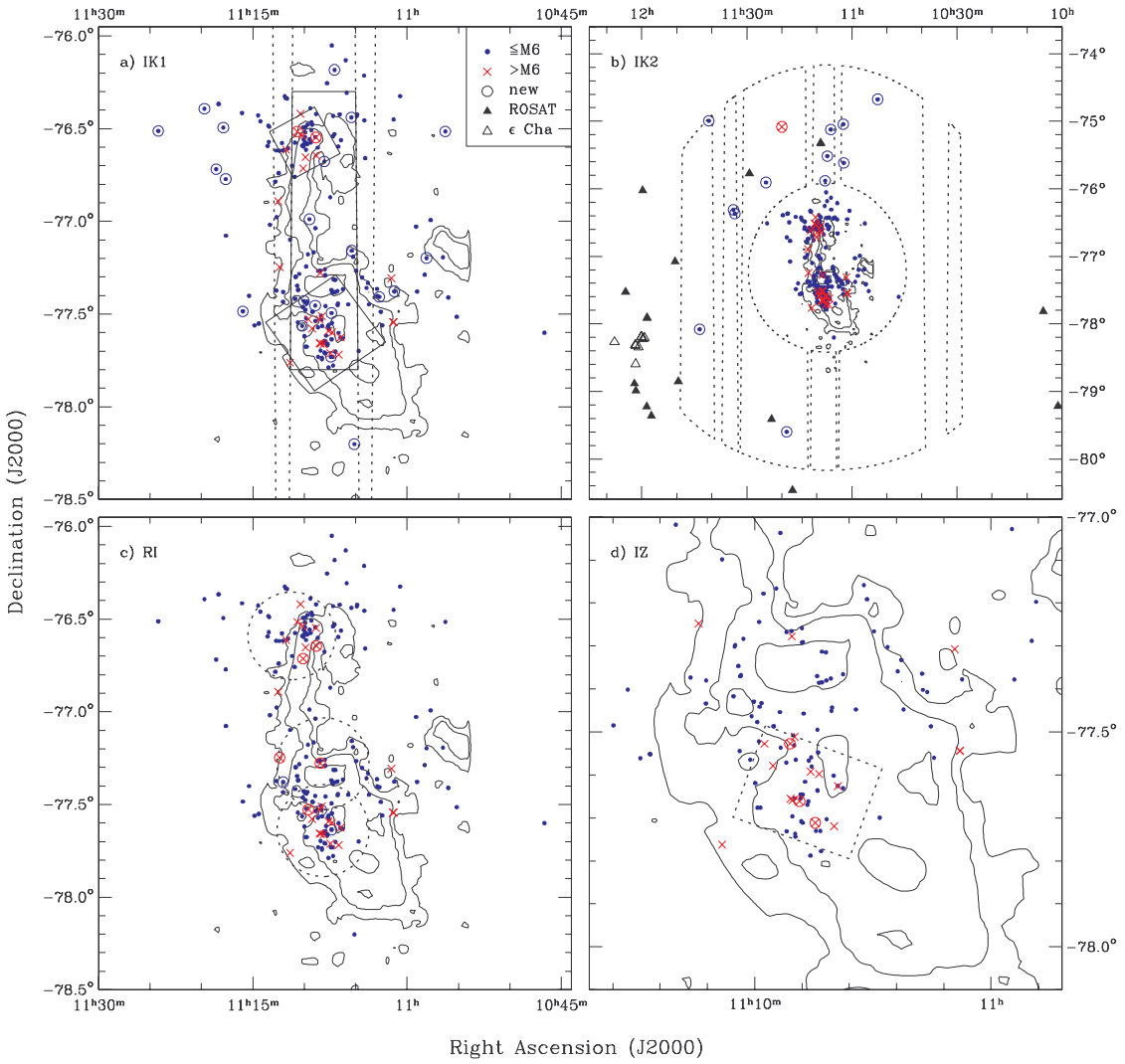


FIG. 1.—Fields in the Chamaeleon I star-forming region that have been searched for new members (*dotted lines*). The known members of the cluster are indicated (*filled circles and crosses*), including the new ones found in this work (*circles*). (*a*) In the IK1 survey (see Fig. 2), the central $1.5^\circ \times 0.35^\circ$ field was searched most thoroughly for new members (*large solid rectangle*). The IMF for this field is shown in Fig. 15. Two narrow strips were not included in this survey because the Second DENIS Release contained no data for them (*dotted lines*). For reference, the fields imaged in X-rays by *Chandra* (Feigelson & Lawson 2004; *upper solid lines*) and *XMM* (Stelzer et al. 2004; *lower solid lines*) are included. (*b*) The IK2 survey (see Fig. 3) applies to the area between $r = 1.25^\circ$–3° from the center of Chamaeleon I for which data are available from the Second DENIS Release (*dotted lines*). This map also includes pre–main-sequence stars identified with *ROSAT* (*filled triangles*; Covino et al. 1997) and probable members of the ϵ Cha young association (*open triangles*, $\tau \sim 6$ Myr; Feigelson et al. 2003; Luhman 2004c). (*c*) The RI survey (see Fig. 4) applies to three fields imaged with IMACS (*dotted lines*). (*d*) The IZ survey (see Figs. 5 and 6) applies to a $0.22^\circ \times 0.28^\circ$ field imaged with ACS (*dotted lines*). The IMF for the ACS field is shown in Fig. 15. The contours represent the extinction map of Cambrésy et al. (1997) at intervals of $A_J = 0.5$, 1, and 2.

masses ($M \sim 0.02\ M_\odot$). A third survey (IK2) considers a small range of masses ($M = 0.2$–$0.02\ M_\odot$) across a very wide field extending well beyond the Chamaeleon I cloud. This survey will be used to measure the spatial distribution of low-mass stars and brown dwarfs. Finally, a very deep survey is performed toward a small field in the center of the southern subcluster in Chamaeleon I (IZ), which will be used to constrain the minimum mass of the IMF. The candidate members identified in this section and observed spectroscopically in § 2.2 are listed in Table 1, which includes all of the relevant photometric measurements.

2.1.1. *IK1 Survey*

For the IK1 survey, I used measurements in J, H, and K_s from the Point Source Catalog of the Two Micron All Sky Survey (2MASS; Skrutskie et al. 2006) and i-band data from the Second Release of the Deep Near-Infrared Survey of the Southern Sky (DENIS; Epchtein et al. 1999) for the area covered by the map of Chamaeleon I in Figure 1*a*. DENIS data are not available within two strips that are indicated in the map. Using these data, I constructed an extinction-corrected diagram of H versus $i - K_s$ in the manner previously done for Chamaeleon I by Luhman (2004a). I defined a boundary that followed the lower envelope of the sequence of previously known members and identified objects above this boundary as candidate members. I have performed spectroscopy on 112 of the ~500 candidates (§ 2.2) and classified them as either members or nonmembers (§ 2.3). These spectroscopic targets and the previously known members appearing in these data are shown in the color-magnitude diagram in Figure 2. When selecting candidates for spectroscopy, I gave highest priority to those that are within the central $1.5^\circ \times 0.35^\circ$ area indicated in Figure 1*a* because I will measure an IMF from members within this field (§ 4). The boundaries of this field were designed to encompass a significant fraction of the known cluster members, which favors a larger area, while minimizing contamination by field stars among the candidates, which favors a smaller area.

TABLE 1

PHOTOMETRY FOR CANDIDATE MEMBERS IN SPECTROSCOPIC SAMPLE

Name	R	I	i[a]	m_{775}	m_{850}	J[b]	H[b]	K_s[b]	J[c]	H[c]	K_s[c]
2M J10314767−7917180	...	...	15.35	...	...	13.41	12.84	12.51	...	...	...
2M J10435748−7633023	...	...	14.73	...	...	12.96	12.39	12.07	...	...	...
2M J10452780−7715335	...	...	11.44	...	...	8.65	7.65	7.17	...	...	...
2M J10523694−7440287	...	...	13.60	...	...	11.45	10.71	10.44	...	...	...
2M J10555824−7418347	...	...	16.39	...	...	13.92	13.34	12.93	...	...	...
2M J10561638−7630530	...	...	14.92	...	...	12.54	11.94	11.52	...	...	...
2M J10580597−7711501	...	...	15.89	...	...	13.40	12.69	12.27	...	...	...
2M J10593228−7753268	...	...	14.96	...	...	13.19	12.61	12.30	...	...	...
2M J11001473−7757103	...	...	12.71	...	...	11.00	10.36	10.04	...	...	...
2M J11011370−7722387	...	...	15.21	...	...	13.06	12.38	12.09	...	...	...
2M J11011926−7732383	...	...	16.59	...	...	13.10	12.22	11.63	...	...	...
2M J11013205−7718249	...	...	17.79	...	...	14.63	14.02	13.54	...	...	...
2M J11014949−7412268	...	...	12.52	...	...	10.18	9.43	8.88	...	...	...
2M J11021927−7536576	...	...	14.09	...	...	12.13	11.54	11.19	...	...	...
2M J11022610−7502407	...	...	13.67	...	...	11.76	11.12	10.81	...	...	...
2M J11024183−7724245	...	...	15.29	...	...	12.80	11.99	11.62	...	...	...
2M J11035902−7743349	13.41	12.42	...	...	...	10.32	9.48	9.05	...	...	...
2M J11045890−7656550	...	...	11.48	...	...	10.13	9.30	9.10	...	...	...
2M J11050005−7728211	22.39	19.97	...	...	...	16.38	14.70	13.95	...	...	...
2M J11050666−7739444	18.73	16.79	16.79	...	...	13.29	11.72	11.03	13.30	11.72	11.00
2M J11050752−7812063	...	...	13.74	...	...	11.78	11.10	10.82	...	...	...
2M J11050937−7706578	12.72	11.70	11.78	...	...	10.27	9.45	9.21	...	...	...
Cha J11051041−7728228	22.26	19.85	...	...	...	...	...	...	...	...	...
2M J11051264−7739070	18.37	16.50	16.55	...	...	13.25	11.88	11.25	13.23	11.89	11.22
2M J11051798−7706565	12.68	11.58	11.67	...	...	9.97	8.93	8.70	...	...	...
2M J11052114−7731541	23.17	20.86	...	...	...	...	15.83	14.61	17.40	15.82	15.07
2M J11052272−7709290	17.61	15.46	15.38	...	...	13.01	12.24	11.87	...	...	...
2M J11052472−7626209	...	...	13.09	...	...	11.47	10.74	10.52	...	...	...
2M J11052489−7620373	...	...	11.61	...	...	10.49	9.81	9.69	...	...	...
2M J11052850−7639489	...	...	11.28	...	...	9.88	9.14	8.87	...	...	...
2M J11053587−7638034	...	...	11.42	...	...	10.18	9.50	9.26	...	...	...
2M J11053731−7738539	21.52	19.53	...	21.18	20.01	15.50	13.97	13.09	15.45	13.86	13.10
2M J11054296−7745213	16.42	14.53	14.38	...	...	11.78	10.62	10.12	...	...	...
2M J11054361−7731525	23.32	20.84	...	...	...	17.09	15.52	14.95	17.16	15.66	14.89
2M J11054371−7729113	22.70	20.18	...	...	...	16.50	15.24	14.43	16.53	15.20	14.42
2M J11054577−7730074	23.04	20.69	...	...	...	16.72	15.21	14.28	16.80	15.30	14.45
Cha J11054699−7737247	...	...	...	25.80	24.14	...	...	...	...	17.33	16.39
2M J11054972−7640462	...	...	11.46	...	...	10.20	9.49	9.25	...	...	...
Cha J11055024−7739268	...	...	...	25.93	24.38	...	...	...	...	18.07	17.09
2M J11055096−7719524	19.87	17.87	17.81	...	...	13.94	12.33	11.57	...	...	...
2M J11055683−7656438	...	...	11.90	...	...	10.64	9.90	9.71	...	...	...
2M J11060010−7507252	...	...	14.15	...	...	12.33	11.75	11.42	...	...	...
2M J11060466−7710063	16.52	14.87	14.88	...	...	13.10	12.35	12.00	...	...	...
2M J11060633−7743443	20.17	18.14	17.94	23.57	22.03	14.19	12.60	11.80	14.19	12.61	11.86
2M J11061896−7729256	23.48	20.82	...	...	...	...	15.69	14.89	17.14	15.60	14.79
Cha J11062045−7743281	...	...	...	25.93	24.41	...	...	...	...	18.11	17.39
2M J11062554−7633418	...	...	15.88	...	...	13.01	12.01	11.49	...	...	...
Cha J11063259−7746281	...	...	...	24.78	23.17	...	...	...	18.55	16.87	16.00
2M J11063479−7645404	...	...	12.65	...	...	11.26	10.60	10.34	...	...	...
Cha J11063721−7740259	...	...	...	25.51	23.90	...	...	...	...	17.48	16.52
2M J11063841−7612032	...	...	10.46	...	...	8.44	7.40	6.99	...	...	...
Cha J11064199−7738330	...	...	...	25.64	24.10	...	...	...	19.20	17.84	16.70
Cha J11064218−7736510	...	...	...	25.97	24.46	...	...	...	...	18.11	17.27
2M J11064235−7632450	...	...	13.61	...	...	11.46	10.35	9.93	...	...	...
2M J11064274−7636124	...	...	11.43	...	...	10.13	9.59	9.35	...	...	...
2M J11064586−7625317	...	...	11.18	...	...	9.91	9.24	9.04	...	...	...
2M J11065939−7530559	...	...	15.79	...	...	13.73	13.14	12.70	...	...	...
2M J11065986−7651181	...	...	10.69	...	...	8.75	7.66	7.32	...	...	...
2M J11070324−7610565	...	...	16.48	...	...	13.85	13.12	12.75	...	...	...
2M J11070350−7631443	...	...	12.95	...	...	11.09	10.09	9.71	...	...	...
2M J11070380−7635440	...	...	10.57	...	...	9.49	8.99	8.73	...	...	...
2M J11072022−7738111	15.94	14.21	...	...	...	8.41	7.70	7.28	...	...	...
2M J11072040−7729403	14.91	13.07	13.00	...	...	11.13	10.55	10.26	...	...	10.14
2M J11072443−7743489	19.55	17.07	16.93	...	...	13.45	12.42	11.84	13.49	12.44	11.86
2M J11072446−7742265	15.90	14.52	14.46	...	...	12.13	11.07	10.64	...	...	10.63

TABLE 1—*Continued*

Name	R	I	i^{a}	m_{775}	m_{850}	J^{b}	H^{b}	K_s^{b}	J^{c}	H^{c}	K_s^{c}
Cha J11072647−7742408	...	...	...	23.30	21.59	...	...	...	17.53	16.45	15.59
2M J11073280−7748594	14.41	13.19	13.15	...	...	11.11	10.05	9.68	...	...	...
2M J11073677−7735167	18.44	16.51	16.33	...	...	12.53	10.72	9.88	12.44	...	9.86
2M J11073737−7733093	19.97	18.04	17.76	...	...	13.64	11.73	10.86	13.59	11.72	10.83
2M J11073832−7747168	16.72	14.70	14.53	...	...	12.24	11.40	11.03	12.24	11.40	10.96
2M J11073840−7552519	...	...	14.66	...	...	12.77	12.12	11.80	...	...	...
2M J11074521−7738049	19.96	17.48	17.22	...	...	11.90	9.42	8.18	...	...	...
2M J11074763−7711156	13.53	12.56	12.60	...	...	10.94	10.12	9.84	...	...	...
2M J11075431−7724571	21.48	19.23	...	...	...	15.99	14.59	14.02	...	...	...
2M J11075613−7421065	...	...	16.06	...	...	13.82	13.19	12.87	...	...	...
2M J11075699−7741558	15.64	14.02	13.93	...	...	11.13	9.77	9.23	...	...	...
2M J11075993−7715317	17.87	15.63	15.45	...	...	12.52	11.65	11.17	...	...	...
2M J11080234−7640343	18.21	15.81	15.46	...	...	12.95	12.31	11.95	12.88	12.32	12.00
2M J11080282−7748375	16.58	15.07	15.02	...	...	12.41	11.11	10.58	...	...	...
2M J11080609−7739406	...	...	...	22.49	20.82	17.36	15.99	15.03	16.91	15.86	15.17
2M J11081069−7637424	13.85	12.87	12.76	...	...	11.20	10.33	10.06	...	...	...
2M J11081241−7719123	22.48	19.64	...	...	...	13.33	10.49	9.07	...	...	...
Cha J11081578−7640198	22.20	19.85	...	...	...	...	...	...	17.95	16.94	16.67
2M J11081916−7656525	...	...	13.65	...	...	11.68	10.69	10.38	...	...	...
Cha J11081938−7731522	22.04	19.64	...	20.85	20.21	...	...	...	17.30	16.49	16.28
2M J11082492−7721579	21.88	19.61	...	...	...	14.75	12.65	11.70	...	...	...
2M J11082570−7716396	23.46	20.75	...	...	...	16.59	15.52	14.40	...	...	...
Cha J11082692−7634482	23.22	20.81	...	...	...	...	...	...	18.36	17.52	16.86
2M J11083016−7728480	23.00	20.60	...	...	...	15.87	14.01	13.07	15.98	14.04	13.06
Cha J11083040−7731387	...	...	...	23.72	22.03	...	...	...	17.84	16.75	15.97
2M J11083897−7614457	...	...	10.87	...	...	9.30	8.31	7.95	...	...	...
2M J11084845−7718233	19.34	17.36	17.19	...	...	13.26	11.46	10.66	...	...	...
2M J11084952−7638443	22.66	19.93	...	...	...	16.08	15.11	14.47	15.96	15.12	14.54
2M J11085176−7632502	20.34	17.77	17.60	...	...	14.29	13.53	12.96	14.30	13.50	12.84
2M J11085527−7704502	...	...	11.61	...	...	9.18	7.94	7.47	...	...	...
2M J11085596−7727132	19.87	17.30	17.08	...	...	13.51	12.29	11.62	...	...	...
2M J11085813−7646392	14.92	13.81	13.65	...	...	11.96	11.20	10.87	...	...	...
2M J11090239−7645196	19.85	17.68	17.48	...	...	15.29	14.60	14.27	...	...	...
2M J11090315−7725584	23.30	20.90	...	...	...	16.25	14.26	13.41	...	...	...
2M J11090332−7700495	...	...	12.17	...	...	9.92	8.86	8.47	...	...	...
2M J11090367−7707456	13.88	12.72	12.79	...	...	10.69	9.69	9.37	...	...	...
2M J11090651−7711246	15.85	14.64	14.63	...	...	12.54	11.66	11.32	...	...	...
2M J11090766−7618144	...	...	9.29	...	...	7.48	6.50	6.18	...	...	...
Cha J11090998−7643570	22.91	20.55	...	...	...	...	...	...	...	...	...
2M J11091379−7637531	13.81	12.69	12.65	...	...	10.88	10.00	9.69	...	...	...
2M J11092068−7713591	14.58	13.12	13.04	...	...	10.38	9.10	8.60	...	...	...
2M J11092482−7642073	15.37	13.93	13.85	...	...	11.35	10.09	9.63	...	...	...
2M J11092582−7726243	16.77	14.82	14.85	...	...	11.35	9.83	9.25	...	...	...
2M J11092913−7659180	...	...	15.70	...	...	13.27	12.51	12.12	...	...	...
2M J11093252−7646573	23.63	20.91	...	...	...	...	15.69	15.01	...	...	...
2M J11093543−7731390	22.39	19.88	...	21.15	19.66	15.94	15.02	14.41	15.92	14.99	14.37
2M J11093719−7726357	18.01	16.10	16.07	...	...	12.70	11.22	10.65	...	...	...
2M J11094525−7740332	17.71	15.43	15.24	...	...	12.36	11.45	11.03	12.36	11.46	...
2M J11094569−7640338	19.75	18.04	18.22	...	...	14.69	13.37	12.68	14.62	13.34	12.63
2M J11094970−7719578	20.52	18.36	...	...	...	14.29	12.53	11.82	...	...	...
2M J11095119−7658568	...	...	10.63	...	...	9.52	8.99	8.79	...	...	...
2M J11095146−7645452	16.44	14.59	14.46	...	...	11.34	9.95	9.36	...	...	...
2M J11095269−7720397	19.61	17.71	17.70	...	...	13.80	12.38	11.60	...	...	...
2M J11095590−7649022	23.04	20.19	...	...	...	15.52	13.51	12.55	...	...	...
2M J11095822−7659147	...	...	13.27	...	...	10.66	9.42	8.96	...	...	...
2M J11095934−7726320	17.50	15.53	15.55	...	...	12.03	10.53	9.89	...	...	...
Cha J11100159−7738052	...	...	...	24.58	22.95	...	...	...	18.68	17.47	16.69
2M J11100192−7725451	20.44	17.80	17.46	...	...	13.83	12.61	12.02	...	...	...
2M J11100653−7643589	21.06	18.79	...	...	...	14.71	13.00	12.26	...	...	...
2M J11100658−7642486	23.27	20.67	...	...	...	16.34	15.86	15.07	...	...	...
2M J11100787−7656425	...	...	16.05	...	...	13.22	11.98	11.43	...	...	...
2M J11101153−7733521	16.33	14.34	14.24	...	...	12.18	11.19	10.78	11.96	...	10.76
2M J11101217−7647250	21.84	19.45	...	...	...	15.19	13.61	12.79	...	...	...
2M J11101233−7727099	17.57	15.70	15.70	...	...	12.41	11.05	10.44	...	...	...
Cha J11102251−7729595	19.10	17.03	...	...	...	...	...	...	...	...	...
2M J11102375−7718212	19.39	17.67	17.65	...	...	14.55	13.40	12.76	...	...	...

TABLE 1—*Continued*

Name	R	I	i[a]	m_{775}	m_{850}	J[b]	H[b]	K_s[b]	J[c]	H[c]	K_s[c]
2M J11102633−7728394	17.51	15.89	15.97	...	...	13.38	12.37	11.88	13.30	12.32	11.75
2M J11102662−7723318	18.34	16.60	16.60	...	...	13.48	12.18	11.61	...	...	...
2M J11102819−7626164	...	...	9.97	...	...	8.44	7.55	7.26	...	...	...
2M J11102990−7736064	14.92	13.72	13.72	...	...	11.65	10.68	10.30	...	...	...
2M J11103031−7701230	...	...	14.54	...	...	12.34	11.52	11.12	...	...	...
2M J11103067−7637186	14.71	13.26	13.21	...	...	10.77	9.57	9.10	...	...	...
2M J11103500−7651257	...	...	17.48	...	...	14.05	12.65	11.92	...	...	...
2M J11103607−7640412	17.51	15.79	15.71	...	...	12.46	10.88	10.20	12.45	...	...
2M J11103749−7722083	22.53	20.01	...	...	...	16.06	14.62	13.85	...	...	...
2M J11104006−7630547	20.55	17.93	17.77	...	...	14.57	13.85	13.34	14.50	13.84	13.40
Cha J11104328−7646280	22.75	20.32	...	...	...	...	...	...	...	...	...
2M J11104343−7641132	17.58	16.02	15.88	...	...	13.04	11.79	11.19	13.11	11.85	11.18
2M J11105038−7631440	12.85	11.94	11.90	...	...	10.32	9.42	9.14	...	...	...
2M J11105076−7718031	16.40	14.45	14.38	...	...	12.04	11.10	10.75	...	...	...
2M J11105215−7709286	13.64	12.40	12.45	...	...	10.28	9.25	8.85	...	...	...
2M J11105705−7713269	20.98	18.73	...	...	...	15.57	14.56	13.87	...	...	...
2M J11110383−7706261	14.98	13.73	13.89	...	...	11.62	10.53	10.19	...	...	...
2M J11110476−7733471	22.60	20.17	...	...	...	16.84	15.76	15.06	...	...	...
2M J11110670−7717594	14.44	13.26	13.33	...	...	11.38	10.43	10.08	...	...	...
2M J11110714−7722056	14.81	13.29	13.38	...	...	10.70	9.54	8.99	...	...	...
2M J11110958−7651505	...	...	16.85	...	...	13.23	11.71	10.92	...	...	...
2M J11111069−7721118	15.75	14.42	14.55	...	...	12.29	11.30	10.88	...	...	...
2M J11111062−7657205	...	...	12.69	...	...	10.32	9.12	8.66	...	...	...
2M J11111311−7732096	22.89	20.53	...	...	...	16.92	15.65	15.08	...	...	...
Cha J11111725−7637008	22.96	20.34	...	...	...	...	...	...	17.16	16.52	16.03
2M J11113045−7712269	16.21	14.71	...	...	...	12.21	11.09	10.63	...	...	...
Cha J11113052−7647467	23.26	20.90	...	...	...	...	...	...	...	...	...
2M J11113409−7729331	19.99	17.71	...	...	...	15.46	14.63	14.04	...	...	...
2M J11113659−7647070	22.90	20.43	...	...	...	16.85	15.90	15.60	...	...	...
2M J11114388−7729437	22.77	20.10	...	...	...	16.96	15.44	14.96	...	...	...
2M J11120288−7722483	18.57	16.26	...	...	...	13.59	12.94	12.51	...	...	...
2M J11122250−7714512	22.22	19.57	...	...	...	15.90	14.93	14.43	...	...	...
2M J11131188−7647392	14.26	13.10	13.13	...	...	11.36	10.46	10.19	...	...	...
Cha J11131563−7647387	23.21	20.85	...	...	...	...	...	...	...	...	...
2M J11132112−7625558	...	...	8.75	...	...	5.44	4.51	4.13	...	...	...
Cha J11140393−7632135	22.10	19.77	...	...	...	...	...	...	...	...	...
2M J11142906−7625399	...	...	14.46	...	...	12.57	11.90	11.61	...	...	...
2M J11152180−7724042	...	...	13.79	...	...	11.76	11.13	10.82	...	...	...
2M J11154549−7724487	...	...	14.72	...	...	12.93	12.39	12.04	...	...	...
2M J11155827−7729046	...	...	13.65	...	...	11.94	11.31	11.02	...	...	...
2M J11173079−7627078	...	...	8.62	...	...	5.56	4.51	4.24	...	...	...
2M J11173792−7646193	...	...	15.85	...	...	13.51	12.95	12.62	...	...	...
2M J11175211−7629392	...	...	13.39	...	...	11.66	11.15	10.71	...	...	...
2M J11183379−7643041	...	...	13.24	...	...	11.34	10.78	10.42	...	...	...
2M J11183572−7935548	...	...	12.20	...	...	10.49	9.89	9.62	...	...	...
2M J11194214−7623326	...	...	14.73	...	...	12.72	12.03	11.72	...	...	...
2M J11195060−7628492	...	...	10.15	...	...	7.52	6.54	5.94	...	...	...
2M J11195652−7504529	...	...	16.68	...	...	14.05	13.33	12.98	...	...	...
2M J11213026−7805240	...	...	12.08	...	...	9.28	8.28	7.85	...	...	...
2M J11225703−7649560	...	...	8.68	...	...	6.20	5.37	5.09	...	...	...
2M J11241186−7630425	...	...	14.87	...	...	12.88	12.30	12.00	...	...	...
2M J11242980−7554237	...	...	12.91	...	...	10.93	10.20	9.88	...	...	...
2M J11253653−7700348	...	...	9.59	...	...	6.41	5.54	5.08	...	...	...
2M J11271677−7816401	...	...	13.41	...	...	11.69	11.14	10.86	...	...	...
2M J11332327−7622092	...	...	12.26	...	...	10.59	10.00	9.71	...	...	...
2M J11334926−7618399	...	...	14.07	...	...	12.15	11.50	11.18	...	...	...
2M J11335700−7807240	...	...	15.92	...	...	13.20	12.58	12.19	...	...	...
2M J11344431−7937063	...	...	15.68	...	...	13.54	12.98	12.61	...	...	...
2M J11404967−7459394	...	...	14.83	...	...	12.68	12.15	11.77	...	...	...
2M J11432669−7804454	...	...	13.61	...	...	11.62	10.97	10.60	...	...	...
2M J11453083−7610479	...	...	14.60	...	...	12.90	12.33	12.00	...	...	...
2M J11455537−7624419	...	...	15.89	...	...	13.77	13.24	12.89	...	...	...

[a] From the Second DENIS Release.
[b] From the 2MASS Point Source Catalog.
[c] Measured with ISPI in this work.

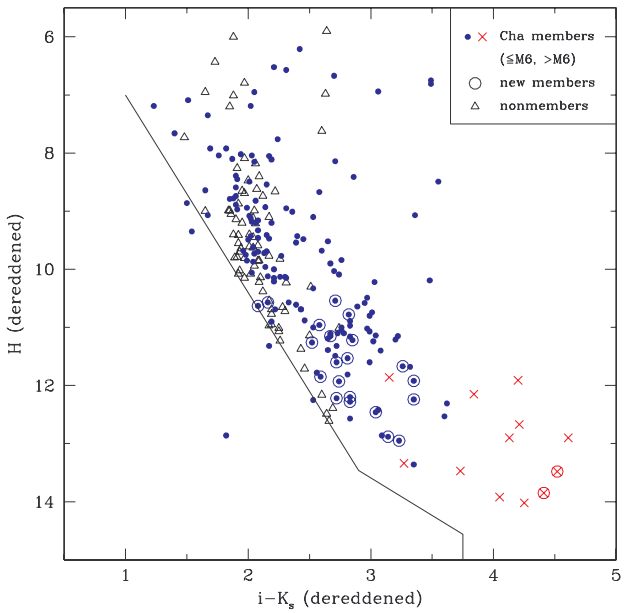


FIG. 2.—Extinction-corrected color-magnitude diagram for the IK1 survey of Chamaeleon I, which applies to the area covered by DENIS in Fig. 1*a*. Candidate members of Chamaeleon I were selected based on positions above the solid boundary and were spectroscopically classified as new members (*open circles*) or nonmembers (*triangles*). All known members within this field are indicated (*filled circles and crosses*). These measurements are from DENIS (*i*) and 2MASS (*H* and K_s).

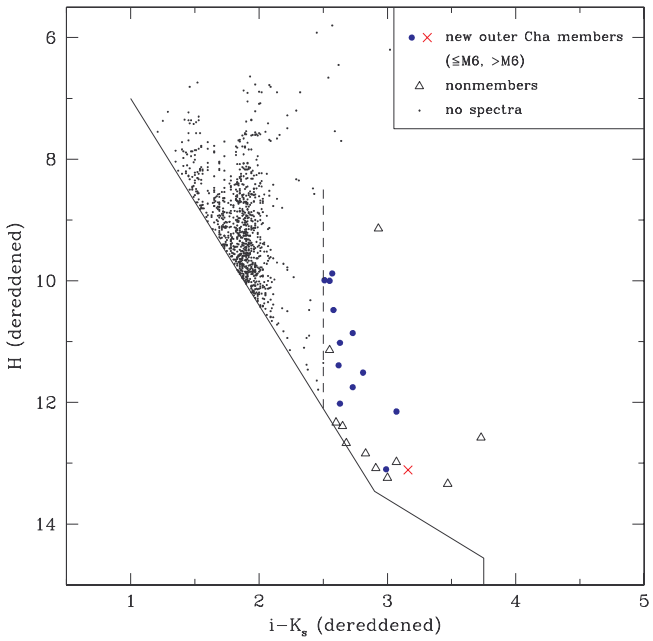


FIG. 3.—Extinction-corrected color-magnitude diagram for the IK2 survey of Chamaeleon I, which applies to the area covered by DENIS in Fig. 1*b*. Candidate low-mass members of Chamaeleon I ($\gtrsim$M4.5, $M \lesssim 0.2\ M_\odot$) were selected based on positions above the solid boundary and right of the dashed line ($I - K_s > 2.5$) and were spectroscopically classified as new members (*circles*) or nonmembers (*triangles*). These measurements are from DENIS (*i*) and 2MASS (*H* and K_s).

Based on the spectral classifications performed in § 2.3, the 112 IK1 candidates that were observed spectroscopically consist of 32 members and 80 nonmembers. Eight of these members were independently discovered by Comerón et al. (2004). In this work, these objects are counted as previously known members rather than new members. The primary in the wide binary brown dwarf 2MASS J11011926−7732383 (hereafter 2M 1101−7732) is also one of the 32 members found during the IK1 survey, but for the purposes of this study, I count it as a previously known member because I presented its discovery in a separate study (Luhman 2004b). Given these considerations, the IK1 survey produced 23 new members.

2.1.2. *IK2 Survey*

To search for low-mass members of Chamaeleon I outside of the area of the IK1 survey, I again used data from the 2MASS Point Source Catalog and the Second DENIS Release. For this wide-field survey, named IK2, I considered the area between radii of 1.25° and 3° from $\alpha = 11^h07^m00^s$, $\delta = -77°10'00''$ (J2000). The map in Figure 1*b* indicates the portion of this annulus for which data are available from the Second DENIS Release. As in the IK1 survey, I constructed an extinction-corrected color-magnitude diagram from the DENIS and 2MASS data and used it to identify candidate members of Chamaeleon I, which are shown on the color-magnitude diagram in Figure 3. Unlike IK1, I selected for spectroscopy only the candidates with $I - K_s > 2.5$, which corresponds to spectral types of $\gtrsim$M4.5 and masses of $M \lesssim 0.2\ M_\odot$. These criteria produced a total of 24 candidate low-mass stars and brown dwarfs. I have obtained spectra of 23 of these candidates (§ 2.2). The remaining object, 2MASS J10504888−7829244, was classified as a galaxy through visual inspection of acquisition images obtained during the spectroscopic observations, and thus a spectrum was unnecessary. I find that 13 of the targets are pre−main-sequence objects (§ 2.3). Kinematic measurements are needed to verify that these sources are directly associated with Chamaeleon I (Covino et al. 1997), but for the purposes of this study, I treat them as members of the star-forming region. The positions of these sources are indicated on the map in Figure 1*b*. For comparison, I also show the positions of other young stars previously detected within the area encompassed by Figure 1*b*. These additional stars consist of probable members of the ϵ Cha association (Feigelson et al. 2003; Luhman 2004c) and pre−main-sequence stars found in the *Röntgensatellit* (*ROSAT*) all-sky survey (Alcalá et al. 1995, 1997; Covino et al. 1997).

2.1.3. *RI Survey*

On the night of 2004 January 11, I obtained *R*- and *I*-band images centered at $\alpha = 11^h08^m10^s$ and $\delta = -77°38'00''$, $\alpha = 11^h08^m10^s$ and $\delta = -77°17'00''$, and $\alpha = 11^h11^m13^s$ and $\delta = -76°35'00''$ (J2000) with the Inamori Magellan Areal Camera and Spectrograph (IMACS) on the Magellan I telescope at Las Campanas Observatory. The instrument contained eight 2048 × 4096 CCDs separated by ∼10″ and arranged in a 4 × 2 mosaic. The plate scale was 0.202″ pixel^{-1}, and the unvignetted field of view was circular with a diameter of 28′. The imaged areas are indicated in the map of Chamaeleon I in Figure 1*c*. In each filter, I obtained two dithered images at each exposure time of 1, 25, and 450 s. Photometry and image coordinates of the sources in these data were measured with `DAOFIND` and `PHOT` under the IRAF package `APPHOT`. Aperture photometry was extracted with a radius of 6 pixels. The background level was measured in an annulus around each source and subtracted from the photometry, where the inner radius of the annulus was 6 pixels, and the width was 1 pixel. The photometry was calibrated in the Cousins system by combining data for standards across a range of colors (Landolt 1992) with the appropriate aperture and airmass corrections. Because an atmospheric dispersion corrector was unavailable at the time of these observations, the image quality varies with position across the images. As a result, the photometric uncertainties

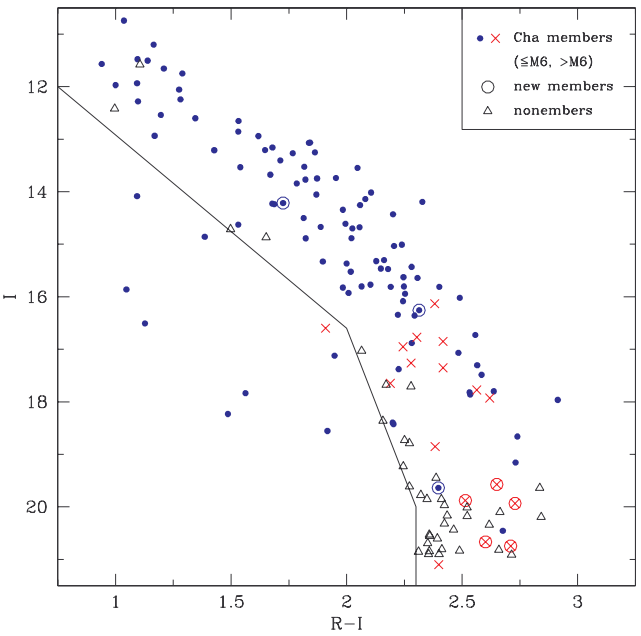


FIG. 4.—Color-magnitude diagram for the RI survey of Chamaeleon I, which applies to the fields imaged with IMACS in Fig. 1*c*. Candidate members of Chamaeleon I were selected based on positions above and right of the solid boundary and were spectroscopically classified as new members (*open circles*) or nonmembers (*triangles*). All known members within this field are indicated (*filled circles and crosses*).

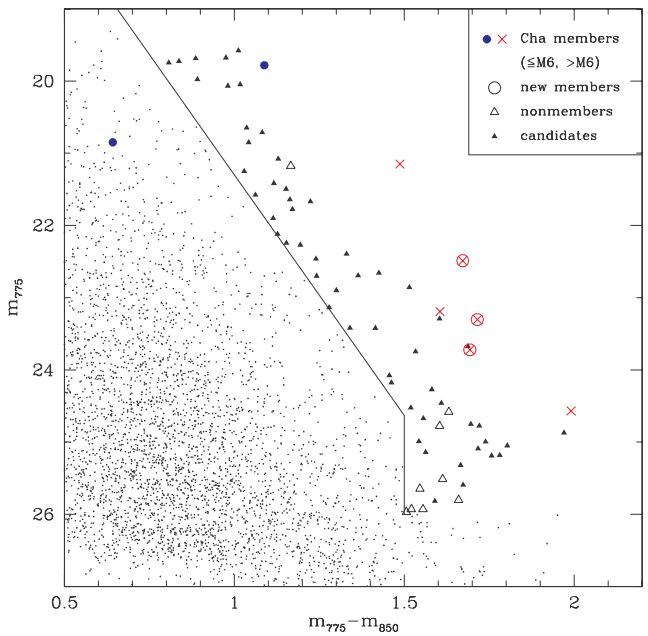


FIG. 5.—Color-magnitude diagram for the IZ survey of Chamaeleon I, which applies to the field imaged with ACS in Fig. 1*d*. Candidate members of Chamaeleon I were selected based on positions above the solid boundaries in this diagram and in Fig. 6. These candidates were spectroscopically classified as new members (*open circles*) or nonmembers (*triangles*). Stars that are candidates members by this diagram but fall below the solid line in Fig. 6 probably have spectral types earlier than M6 and are either field stars or reddened stellar cluster members (*filled triangles*). Stars that are too faint to be reliably identified as either field stars or candidate members ($m_{775} > 26$) have been excluded from this analysis. All unsaturated, known members within this field are indicated (*filled circles and crosses*).

for these data are relatively large, with a minimum value of $\sim$0.1 mag.

As in the IK1 and IK2 color-magnitude diagrams, I defined a boundary that follows the lower envelope of the sequence of known members in I versus $R - I$ for separating probable field stars from candidate members of Chamaeleon I. I have obtained spectra of 46 of the 116 resulting candidates (§ 2.2), which are classified as 38 nonmembers and eight members (§ 2.3). Figure 4 shows the color-magnitude diagram of these 46 sources and the previously known members that have unsaturated IMACS photometry. The positions of the new members from the RI survey are indicated on the map in Figure 1*c*.

2.1.4. *IZ Survey*

To search for members of Chamaeleon I at very low masses ($M \sim 0.01\ M_{\odot}$), I used deep optical and near-IR images of the densest portion of the southern subcluster that were obtained by Luhman et al. (2005c). The optical images were collected with the Advanced Camera for Surveys (ACS) aboard *HST* through the F775W and F850LP filters, which are similar to the i' and z' filters from the Sloan Digital Sky Survey (Sirianni et al. 2005). These images covered a $0.22^{\circ} \times 0.28^{\circ}$ area, which is indicated in Figure 1*d*. The near-IR imaging was performed with the Infrared Side Port Imager (ISPI) at the 4 m Blanco telescope at CTIO through the J, H, and K_s filters. These data covered a $20' \times 20'$ area and were centered at $\alpha = 11^{\rm h}07^{\rm m}45^{\rm s}$, $\delta = -77^{\circ}38'20''$ (J2000), completely encompassing the ACS field.

In Figure 5, I plot a color-magnitude diagram consisting of photometry at F751W and F850LP for all unsaturated sources in the ACS images. The saturation limits of these data correspond to masses that are below the hydrogen-burning limit for unreddened members of Chamaeleon I. In fact, most of the known substellar members of the cluster ($\gtrsim$M6) are saturated. Two members with spectral types earlier than M6 are not saturated because one of them, ISO 79, has significant reddening and the other star, Cha J11081938−7731522, is subluminous for its color and spectral type and thus may be seen in scattered light (Appendix A). To separate candidate cluster members and probable field stars, I defined a boundary below the lower envelope of the sequence of known members. Because the $I - Z$ colors of late-type field dwarfs do not decrease significantly from late-M to mid-L (Steele & Howells 2000; Dahn et al. 2002; Dobbie et al. 2002), I have made this boundary vertical at the reddest colors. At $m_{775} > 26$, I cannot use Figure 5 to reliably separate field stars and candidate members because the photometric uncertainties are too large. Considering only stars at $m_{775} \leq 26$, I found 69 candidates in Figure 5.

Color-color diagrams like $I - K$ versus $J - H$ can further refine samples of candidate late-type objects found in color-magnitude diagrams (Luhman 2000). Therefore, I constructed an analogous diagram of $m_{775} - K_s$ versus $J - H$ in Figure 6 by combining the ACS and ISPI photometry. To identify objects in this diagram that have colors indicative of late spectral types, I have defined a boundary in Figure 6 that approximates the reddening vector for a spectral type of M6, which corresponds to $M \sim 0.1\ M_{\odot}$ for members of Chamaeleon I. The slope of this vector was determined from the distribution of reddened stars in Figure 6. The origin of the vector is placed at $J - H = 0.56$ (Leggett 1992) and a value of $m_{775} - K_s$ such that the vector is slightly redder than the color of the known member ISO 79 (M5.25; Luhman 2004a). Objects later than M6 should appear above this reddening vector. Among the 69 candidates from Figure 5, 57 sources have photometry in J, H, and K_s and thus are present in Figure 6. Eight of these 57 objects are above the reddening vector, indicating that they could be later than M6. The 49 candidates below the vector are unlikely to be substellar members, but some of them could be

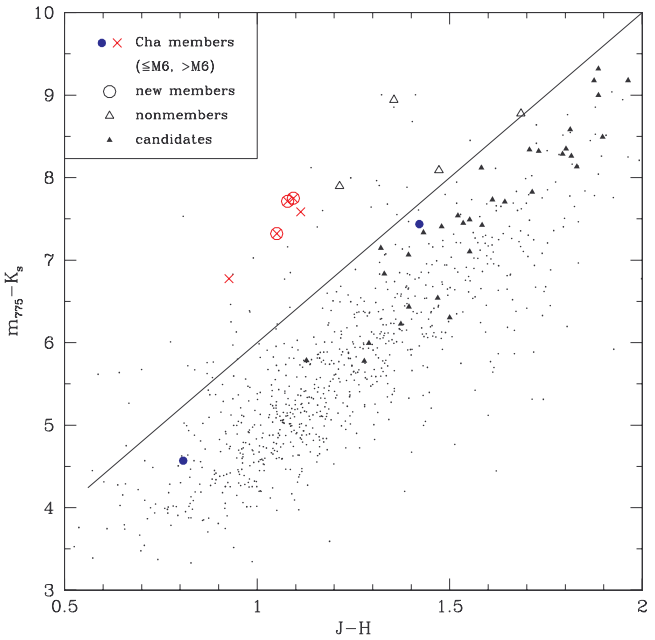


FIG. 6.—Color-color diagram for the IZ survey of Chamaeleon I, which applies to the field imaged with ACS in Fig. 1*d*. The symbols are the same as in Fig. 5.

young stars with very high reddenings. One of the eight late-type candidates, Cha 110913−773444, also exhibits mid-IR excess emission in images from the *Spitzer Space Telescope*. Based on the promising position of this object in Figures 5 and 6 and its mid-IR excess, Luhman et al. (2005c) obtained a spectrum of this object and confirmed its youth and late-type nature. I have performed spectroscopy on the seven remaining late-type candidates from Figure 6 (§ 2.2), three of which are confirmed as low-mass members of Chamaeleon I (§ 2.3). I have also obtained spectra of 6 of the 12 candidates from Figure 5 that lack JHK_s photometry and thus could not be plotted in Figure 6. One of these six objects was not detected by ISPI because it is close to a brighter stellar member, CHXR 73. Spectroscopic confirmation of this probable companion was presented by Luhman et al. (2006). The five remaining ACS-only candidates in my spectroscopic sample are nonmembers (§ 2.3).

2.2. *Spectroscopy*

I performed optical and near-IR spectroscopy on 193 candidate members of Chamaeleon I that were identified in § 2.1 and 53 miscellaneous targets that are described in this section. Some of these objects were observed multiple times. Table 2 summarizes the dates, telescopes, and instrument configurations for these observations. In this section, I provide additional details of the target selection and observations. The identity of the sources in each of the categories of targets described below can be found in Tables 3 and 4, which list the basis of selection for each target.

I observed one of the IK1 candidates with the Magellan Inamori Kyocera Echelle (MIKE). The details of the observations are the same as those described by Muzerolle et al. (2005) for other targets observed on that same night. During the IMACS observations in 2004 January, I obtained long-slit and multiobject spectra of 123 sources, consisting of 85 IK1 candidates, 19 known members of Chamaeleon I that I have not previously classified, four candidate members from López Martí et al. (2004), six candidate brown dwarfs from 2MASS data, two objects with uncertain previous classifications that were noted by Luhman (2004a), six X-ray sources from Feigelson & Lawson (2004), and a candidate companion to the binary ISO 250 (López Martí et al. 2004). The 2MASS brown dwarf candidates were selected to have uncertainties less than 0.1 mag in J, H, and K_s, $0.5 \leq J - H \leq 1$, $H - K_s > 0.3$, and positions in the central $1.5^\circ \times 0.35^\circ$ area indicated in Figure 1*a*. The 2MASS candidates, X-ray sources, stars with uncertain classifications, and the candidate companion are all classified as nonmembers in § 2.3.

During the observations with the Low Dispersion Survey Spectrograph (LDSS-2) on the Magellan II telescope at Las Campanas Observatory on the night of 2004 March 31, I obtained long-slit spectra of 18 and 23 candidates from the IK1 and IK2 surveys, respectively. The one remaining IK2 candidate was not observed spectroscopically because it was identified as a galaxy on acquisition images obtained with LDSS-2, as discussed in § 2.1.2. On the nights of 2004 April 26 and 27, I performed long-slit spectroscopy on eight IK1 candidates and multislit spectroscopy on

TABLE 2
SPECTROSCOPY OBSERVING LOG

Night	Date	Telescope + Instrument	Disperser	λ (μm)	$\lambda/\Delta\lambda$
1.....	2004 Jan 2	Magellan II + MIKE	...	0.5–1	20000
2.....	2004 Jan 7	Magellan I + IMACS	200 grism	0.5–1	900
3.....	2004 Jan 8	Magellan I + IMACS	200 grism	0.5–1	900
4.....	2004 Jan 9	Magellan I + IMACS	200 grism	0.5–1	900
5.....	2004 Jan 10	Magellan I + IMACS	200 grism	0.5–1	900
6.....	2004 Jan 11	Magellan I + IMACS	200 grism	0.5–1	900
7.....	2004 Mar 31	Magellan II + LDSS-2	Med. red grism	0.48–0.92	600
8.....	2004 Apr 26	Magellan I + IMACS	200 grism	0.5–1	900
9.....	2004 Apr 27	Magellan I + IMACS	200 grism	0.5–1	900
10.....	2005 Jan 2	Magellan I + IMACS	200 grism	0.5–1	1500
11.....	2005 Jan 3	Magellan I + IMACS	200 grism	0.5–1	900
12.....	2005 Jan 4	Magellan I + IMACS	200 grism	0.5–1	900
13.....	2005 Jan 5	Magellan I + IMACS	200 grism	0.5–1	900
14.....	2005 Jan 6	Magellan I + IMACS	200 grism	0.5–1	900
15.....	2005 Mar 23	Gemini + GNIRS	31.7 cross-dispersed	1–2.5	2000
16.....	2005 Mar 24	Gemini + GNIRS	31.7 cross-dispersed	1–2.5	2000
17.....	2005 Mar 25	Gemini + GNIRS	31.7 cross-dispersed	1–2.5	2000

TABLE 3
NEW MEMBERS OF CHAMAELEON I

2MASS[a]	Name[b]	Spectral Type[c]	Membership Evidence[d]	Basis of Selection[e]	Night
J10523694−7440287	...	M4.75	NaK	IK2	7
J10561638−7630530	ESO Hα 553	M5.6	NaK, e	IK1	4
J10580597−7711501	...	M5.25	NaK	IK1	4
J11011370−7722387	...	M5.25	NaK	IK1	7
J11021927−7536576	...	M4.5	NaK	IK2	7
J11022610−7502407	...	M4.75	NaK	IK2	7
J11024183−7724245	[LM04] 423	M5	NaK, A_V	IK1	7
J11050752−7812063	...	M4.75	NaK	IK1	7
J11052272−7709290	...	M4.75	NaK, A_V	IK1	3
J11052472−7626209	...	M2.75	NaK	IK1	5
J11060010−7507252	...	M4.5	NaK	IK2	7
J11065939−7530559	...	M5.25	e, NaK	IK2	7
J11070324−7610565	...	M6	NaK	IK1	5
J11072022−7738111[f]	...	M4.25	NaK, A_V	RI	14
J11072040−7729403	[LM04] 448,ISO 99	M4.5	NaK	IK1	2
J11072443−7743489	[LM04] 429	M5.75	NaK, A_V	IK1	2
...	Cha J11072647−7742408	≥M9	H_2O	IZ	15, 17
J11073840−7552519	...	M4.75	NaK	IK2	7
J11080234−7640343	[LM04] 717	M6	NaK	IK1	2
J11080609−7739406	...	≥M9	H_2O	IZ	15
...	Cha J11081938−7731522	M4.75	NaK, ex	RI	8
J11082570−7716396	...	M8	NaK, ex	RI	8
...	Cha J11083040−7731387	≥M9	H_2O	IZ	15, 17
J11084952−7638443	...	M8.75	e, NaK, ex	RI	9, 11, 12
J11085176−7632502	[LM04] 737	M7.25	NaK, A_V	IK1	5, 11, 12
J11085596−7727132	ISO 167	M5.25	NaK, A_V	IK1	2
J11092913−7659180	[LM04] 602	M5.25	NaK, A_V	IK1	2
J11093543−7731390	...	M8.25	NaK	RI	8
J11100192−7725451	[LM04] 419	M5.25	NaK, A_V	IK1	2
J11100658−7642486	...	M9.25	NaK	RI	9, 11, 12
J11101153−7733521	...	M4.5	NaK, A_V	IK1	2
J11104006−7630547	...	M7.25	NaK, A_V	IK1	5
J11112249−7745427	[LM04] 436	M8.25	NaK, ex	LM04	2
J11114533−7636505	[LM04] 743	M8	NaK, ex	LM04	2, 11, 12
J11120288−7722483	...	M6	A_V, NaK	RI	9
J11122250−7714512	...	M9.25	NaK	RI	9, 11, 12, 13
J11123099−7653342	[LM04] 601	M7	NaK	LM04	2
J11155827−7729046	...	M4.5	NaK	IK1	7
J11173792−7646193	...	M5.75	NaK	IK1	4, 5
J11175211−7629392	...	M4.5	NaK	IK1	7
J11183379−7643041	...	M5	NaK	IK1	7
J11183572−7935548	...	M4.75	e, NaK	IK2	7
J11194214−7623326	...	M5	NaK	IK1	7, 8
J11195652−7504529	...	M7.25	NaK	IK2	7
J11241186−7630425	...	M5	NaK, A_V	IK1	8
J11242980−7554237	...	M4.75	NaK	IK2	7
J11332327−7622092	...	M4.5	NaK	IK2	7
J11334926−7618399	...	M4.5	NaK	IK2	7
J11404967−7459394	...	M5.75	NaK	IK2	7
J11432669−7804454	...	M5	e, NaK	IK2	7

[a] From the 2MASS Point Source Catalog.
[b] Sources that are not in the 2MASS Point Source Catalog have been assigned coordinate-based identifications.
[c] Uncertainties are ±0.25 subclass unless noted otherwise.
[d] Membership in Chamaeleon I is indicated by $A_V \gtrsim 1$ and a position above the main sequence for the distance of Chamaeleon I ("A_V"), strong emission lines ("e"), Na I and K I strengths intermediate between those of dwarfs and giants ("NaK"), IR excess emission ("ex"), or the shape of the gravity-sensitive steam bands ("H_2O").
[e] Sources were selected for spectroscopy because they appeared as candidate members in Figs. 2 ("IK1"), 3 ("IK2"), 4 ("RI"), or 5 ("IZ"), or were identified as candidate members by López Martí et al. (2004) ("LM04").
[f] Possible wide companion to T26 (Reipurth & Zinnecker 1993; Ghez et al. 1997).

37 RI candidates. One of these IK1 candidates was also observed during an earlier run. During the IMACS observations in 2005 January, I obtained long-slit and multislit spectra of 32 targets, consisting of one IK1 candidate, nine RI candidates, a candidate companion to KG 102 (Persi et al. 2005), one star with an uncertain previous classification, eight candidates identified with mid-IR photometry from the *Spitzer Space Telescope*, five known members that I have not previously classified, and seven targets observed in earlier runs that needed a better signal-to-noise ratio. Although it lacks previous spectroscopic confirmation of

TABLE 4

NONMEMBERS

2MASS[a]	Name[b]	Spectral Type[c]	Basis of Selection[d]	Night
J10314767−7917180	...	M5.25 V	IK2	7
J10435748−7633023	...	M4.75 V[e]	IK2	7
J10452780−7715335	...	M6 III	IK1	9
J10555824−7418347	...	M7.5 V[e]	IK2	7
J10593228−7753268	...	M4.75 V	IK1	7
J11001473−7757103	...	<K0	IK1	7
J11014949−7412268	...	Giant	IK2	7
J11035902−7743349	ISO 35	<K0	RI	14
J11045890−7656550	...	Giant	IK1	4
J11050005−7728211	...	<M0	RI	8
J11050666−7739444	ISO 57	<M0	IK1	1
J11050937−7706578	...	Giant	IK1	3
...	Cha J11051041−7728228	Galaxy	RI	8
J11051264−7739070	ISO 58	Giant	IK1	2
J11051263−7742151	...	<M0	2M	2
J11051798−7706565	...	Giant	RI	14
J11052114−7731541	...	<M0	RI	8
J11052489−7620373	...	Giant	IK1	5
J11052850−7639489	...	Giant	IK1	4
J11053587−7638034	...	Giant	IK1	4
J11053731−7738539	...	K0 V	IZ	16
J11054296−7745213	ISO 64	Giant	IK1	2
J11054361−7731525	...	<M0	RI	8
J11054371−7729113	...	M3 V	RI	8
J11054577−7730074	...	<M0	RI	8
...	Cha J11054699−7737247	<M0	IZ	16
J11054972−7640462	...	Giant	IK1	4
...	Cha J11055024−7739268	<M0	IZ	16
J11055096−7719524	ISO 67	Giant	IK1	3
...	Cha J11055362−7638533	<M0	IRAC	10
J11055683−7656438	...	Giant	IK1	4
J11060466−7710063	...	M3.25 V	RI	14
J11060633−7743443	ISO 73	<M0	IK1	2
J11061896−7729256	...	<M0	RI	8
...	Cha J11062045−7743281	<M0	IZ	16
...	Cha J11063259−7746281	M5−M7 V?	IZ	15
J11063479−7645404	...	Giant	IK1	2
...	Cha J11063721−7740259	<M0	IZ	17
J11063841−7612032	...	Giant	IK1	5
...	Cha J11064199−7738330	<M0	IZ	15
...	Cha J11064218−7736510	<M0	IZ	16
J11064235−7632450	...	Giant	IK1	5
J11064274−7636124	...	Giant	IK1	5
J11064586−7625317	...	Giant	IK1	5
J11065986−7651181	...	Giant	IK1	7
J11070350−7631443	...	Giant[f]	IK1	5
J11070380−7635440	...	Giant	IK1	4
J11070483−7652432	...	M0	2M	2
J11072446−7742265	...	Giant	IK1	2
J11073280−7748594	ISO 104	Giant	IK1	2
J11073677−7735167	Cam2-26, ISO 107	Giant	IK1	2
J11073737−7733093	Cam2-27, ISO 109	Giant	IK1	2
J11074521−7738049	ISO 113	Giant	IK1	2
J11074763−7711156	...	Giant	IK1	3
J11075431−7724571	...	M3 V	RI	8
J11075613−7421065	...	M5.75 V	IK2	7
J11075699−7741558	ISO 118	Giant	IK1	2
J11080282−7748375	ISO 125	Giant	IK1	2
J11081069−7637424	...	Giant	IK1	2, 5
J11081204−7622124	...	Galaxy	IRAC	14
J11081241−7719123	Cam2-34, [LM04] 420, ISO 131	Carbon[g]	RI	8
...	Cha J11081578−7640198	M0 V	RI	9
J11081916−7656525	ISO 139	Giant	IK1	2
J11082492−7721579	ISO 146	<M0	RI	8
...	Cha J11082692−7634482	M2−M4 V	RI	9
J11083016−7728480	...	<M0	RI	8

TABLE 4—*Continued*

2MASS[a]	Name[b]	Spectral Type[c]	Basis of Selection[d]	Night
J11083897−7614457	...	Giant	IK1	5
J11084845−7718233	ISO 155	Giant	IK1	3
J11085135−7638262	...	K5−K6	X-ray	5
J11085527−7704502	ISO 166	Giant	IK1	3
J11085651−7645154	...	Giant	IRAC	11, 12
J11085759−7645151	...	<K0	2M	2
J11085813−7646392	ISO 170	Giant	IK1	2
J11090239−7645196	...	M4.5 V	RI	9
J11090315−7725584	...	<M0	RI	8
J11090332−7700495	ISO 172	Giant	IK1	2, 3
J11090367−7707456	ISO 175	Giant	IK1	3
J11090651−7711246	ISO 176	Giant	IK1	3
J11090766−7618144	...	Giant	IK1	4
...	Cha J11090998−7643570	M1-M3 V	RI	9
J11091011−7627113	...	Mid-K	X-ray	5
J11091058−7632508	Cam2-36	<M0[g]	Unc	5
J11091336−7630232	...	<M0	X-ray	5
J11091379−7637531	ISO 183	Giant	IK1	2, 5
J11092068−7713591	ISO 188	Giant	IK1	3
J11092482−7642073	ISO 191	Giant	IK1	7
J11092582−7726243	ISO 190	Giant	IK1	2, 3
J11092956−7702052	...	<M0	2M	3
J11093252−7646573	...	M4 V	RI	9
J11093719−7726357	ISO 195	Giant	IK1	3
J11094569−7640338	...	Giant	IK1	2
...	KG 102B	Giant	Comp	13
J11094970−7719578	ISO 210	<M0	RI	8, 9
J11095119−7658568	ISO 213	Giant	IK1	4
J11095146−7645452	[LM04] 721, ISO 214	Giant	IK1	2
J11095269−7720397	ISO 219	<K0	IK1	3
J11095300−7730588	SGR 1	<M0	Unc	11, 12
J11095465−7625333	...	Giant	X-ray	5
J11095590−7649022	...	<M0	RI	9
J11095822−7659147	[LM04] 616, ISO 229	Giant	IK1	2
J11095934−7726320	ISO 230	Giant	IK1	2, 3
...	Cha J11100159−7738052	M9−L1 V?	IZ	15
J11100653−7643589	...	Giant	RI	9
J11100787−7656425	ISO 236	Giant	IK1	2
J11101217−7647250	...	<M0	RI	11, 12
J11101233−7727099	ISO 239	Giant	IK1	2
...	Cha J11102251−7729595	<K0	RI	8
J11102375−7718212	...	Giant	IK1	7, 11, 12
J11102633−7728394	...	<K0	IK1	2
J11102662−7723318	...	Giant	IK1	2, 3
J11102819−7626164	ISO 242	Giant	IK1	4
J11102990−7736064	ISO 243	Giant	IK1	7
J11103031−7701230	...	Giant	IK1	2
J11103067−7637186	ISO 245	Giant	IK1	2
J11103500−7651257	...	<K0	IK1	2
J11103607−7640412	ISO 249	Giant	IK1	2
...	ISO 250 candidate companion	M2−M4	Comp	6
J11103749−7722083	...	<M0	RI	11, 12
J11104082−7740525	...	Giant	2M	2
J11104290−7634048	OTS 61	<M0	Unc	2, 5
...	Cha J11104328−7646280	M3.5 V	RI	9
J11104343−7641132	ISO 253	Giant	IK1	2
J11104343−7702221	...	<M0	2M	2
J11105038−7631440	ISO 255	Giant	IK1	5
J11105185−7642259	...	<M0	IRAC	11, 12
J11105215−7709286	ISO 257	Giant	IK1	3
J11105353−7726389	...	Giant	IRAC	11, 12
J11105705−7713269	...	M4 V	RI	9
J11110383−7706261	ISO 263	Giant	IK1	4
J11110476−7733471	...	M3 V	RI	8
J11110670−7717594	ISO 264	Giant	IK1	3
J11110714−7722056	ISO 265	Giant	IK1	3
J11110958−7651505	ISO 266	Giant	IK1	7

TABLE 4—*Continued*

2MASS[a]	Name[b]	Spectral Type[c]	Basis of Selection[d]	Night
J11111069−7721118	ISO 268	Giant	IK1	3
J11111062−7657205	ISO 267	Giant	IK1	2
J11111311−7732096	...	M3 V	RI	8
J11111680−7628573	...	<K0	X-ray	5
...	Cha J11111725−7637008	M8 V	RI	9
J11111985−7638264	...	M3−M4	X-ray	2
...	Cha J11112420−7637434	<M0	IRAC	11, 12
J11113045−7712269	ISO 276	Giant	RI	14
...	Cha J11113052−7647467	<M3	RI	9
J11113409−7729331	...	M5.5 V	RI	11, 12, 13
J11113659−7647070	...	M3.5 V	RI	9
J11114388−7729437	...	M2 V	RI	8
...	Cha J11114773−7642167	Galaxy	IRAC	11, 12
J11115884−7730376	[LM04] 401	<M4	LM04	2
...	Cha J11130714−7638575	<M0	IRAC	11, 12
J11131188−7647392	...	Giant	IK1	2
...	Cha J11131563−7647387	Mid-M?	RI	9
J11132112−7625558	...	M6 III	IK1	14
...	Cha J11140393−7632135	M5.5 V	RI	11, 12
J11154549−7724487	ESO Hα 573	M4.75 V[h]	IK1	7
J11173079−7627078	...	M3 III	IK1	9
J11195060−7628492	...	M8.5 III	IK1	9
J11213026−7805240	...	M6 III	IK1	9
J11225703−7649560	...	K5 III	IK1	9
J11253653−7700348	...	M	IK1	9
J11271677−7816401	...	M4.75 V	IK2	7
J11335700−7807240	...	M8 V	IK2	7
J11344431−7937063	...	M5.75 V	IK2	7
J11453083−7610479	...	M4.25 V	IK2	7
J11455537−7624419	...	M5 V	IK2	7

[a] From the 2MASS Point Source Catalog.
[b] Sources that are not in the 2MASS Point Source Catalog have been assigned coordinate-based identifications.
[c] Uncertainties are ±0.25 subclass unless noted otherwise.
[d] Sources were selected for spectroscopy because their previous classifications were uncertain ("Unc"), they were previously identified candidate companions ("Comp"), they were candidate members based on Figs. 2 ("IK1"), 3 ("IK2"), 4 ("RI"), 5 ("IZ"), 2MASS photometry ("2M"), *Spitzer* photometry ("IRAC"), or X-ray emission ("X-ray"), or they were identified as candidate members by López Martí et al. (2004) ("LM04").
[e] Spectral features suggest a surface gravity intermediate between those of Chamaeleon I members and field dwarfs.
[f] Classified as a background giant by Brandner & Zinnecker (1997).
[g] Classified as an M-type member of Chamaeleon I by Gómez & Mardones (2003).
[h] Classified as M5.5 V by Comerón et al. (2004).

youth and membership, I am counting the companion T39B as one of the known members. To provide sufficiently high spectral resolution for the measurement of Li absorption in this possible companion, it was observed with the 600 line mm^{-1} grism, which provided coverage of 0.6–0.92 μm and a resolution of $R = 5000$. All other targets were observed with the instrument configuration that is indicated in Table 2. The *Spitzer* candidates were identified with data from Luhman et al. (2005b) using the color criteria described in that study. Finally, on the nights of 2005 March 23–25, I obtained near-IR spectra of 12 IZ candidates with the Gemini Near-Infrared Spectrograph (GNIRS) at Gemini South Observatory through program GS-2005A-C-13. The observing and analysis procedures were the same as those described by Luhman et al. (2004) for spectroscopy of OTS 44.

2.3. *Classification of Candidate Members*

To measure spectral types and assess membership in Chamaeleon I for the 246 targets in my spectroscopic sample, I applied the classification methods developed in my previous studies of this kind (Luhman 1999, 2004a, 2006; Luhman et al. 2003b). In brief, spectral types were measured from the optical spectra by comparing them to the averages of dwarfs and giants and to spectra of previously classified members of Chamaeleon I (Luhman 2004a), while the IR spectra were classified through comparison to IR data for optically classified young objects (Luhman et al. 2004). To evaluate the membership of each target, I employed various diagnostics based on the spectra, photometry, and other published data, which included gravity-sensitive lines, emission lines, IR excess emission, Li absorption, reddening, and radial velocities.

I have classified 50 targets as new members of Chamaeleon I and 163 targets as nonmembers. The remaining 33 objects in my spectroscopic sample are previously known members. The new members, nonmembers, and previously known members are listed in Tables 3, 4, and 5, respectively. The source 2M J1101−7732 is counted as a previously known member and is omitted from Table 5 because it was already presented by Luhman (2004b), but the photometry used for its selection is included in Table 1. Tables 3–5 provide the source identifications, the available spectral types, the basis for each object's selection for spectroscopy, the night on which it was observed, and its evidence of membership or nonmembership. The references for the membership data consist of Luhman (2004a), Comerón et al. (2004), Luhman et al. (2005b), this work, and unpublished *Spitzer* data. For sources that

TABLE 5
PREVIOUSLY KNOWN MEMBERS OF CHAMAELEON I WITH NEW SPECTROSCOPY

2MASS[a]	Name	Spectral Type[b]	Ref.	Membership Evidence[c]	Night
J10550964−7730540	ESO Hα 552	M5, M4.5	1, 2	NaK	10
J10555973−7724399	T3A	M1, M0.5, M0.5, K8−M0.5	3, 4, 5, 2	e, ex, rv, A_V	4
. . .	T3B	M3.5	2	NaK	4
J11013205−7718249[d]	ESO Hα 554	M8.5, M8	1, 2	NaK	5
J11062554−7633418[d]	ESO Hα 559	M6, M5.25	1, 2	NaK, e, A_V, ex	5
J11065906−7718535	T23	M1.5, M4.25	6, 2	e, ex, NaK	4
J11070925−7718471	ISO 91	M2.5, M2−M4	7, 2	ex	3
J11072825−7652118	T27	K0:, M1, M1.5, M1.5+M3, M3	3, 4, 5, 8, 2	e, ex, rv, Li	4
J11073832−7747168[d]	ESO Hα 560	M5, M4.5	1, 2	NaK, A_V	2
J11074366−7739411	T28	M0.5, M0.5, M1, M0	4, 6, 9, 2	e, ex, A_V	2
J11075792−7738449	T29	K7, K4−K6	9, 2	e, ex, A_V	2
J11075809−7742413	T30	M2.5, M2.5	9, 2	e, Li, rv, A_V, ex	2
J11075993−7715317[d]	ESO Hα 561	M6.5, M5.75	1, 2	NaK, A_V	3
J11084069−7636078	CHXR 33	M0, M0, M2.5	10, 11, 2	Li, A_V	2, 5
. . .	T39B[e]	M3	2	Li	13
J11091769−7627578	CHXR 37	K7	12, 13, 2	Li, rv, A_V	5
J11092379−7623207	T40	K6	5, 2	e, ex, Li, rv, A_V	5
J11094192−7634584	C1-25	<M0	2	ex	2
J11094525−7740332[d]	ESO Hα 566	M6.5, M5.75	1, 2	NaK, A_V	2
J11094918−7731197	KG 102	M6, M5.5, M5.5	14, 15, 2	e, NaK	2, 13
J11095505−7632409	C1-2	<M0	2	ex, e	5
J11095873−7737088	T45	K0:, K7−M0, K7−M0, M1.25	3, 4, 5, 2	e, ex	2
J11100469−7635452	T45a	M0, M1	5, 2	e, ex	2
J11100704−7629376	T46	K2:, K7, M0, M0	3, 4, 5, 2	e, ex, rv, A_V	5
J11100934−7632178	OTS 44	≥M9.5 ,M9.5	16, 2	H_2O, ex, NaK	13
J11105076−7718031[d]	ESO Hα 568	M4.5, M4.25	1, 2	NaK, A_V	7
J11105333−7634319	T48	M1, M1:, M3.75	4, 5, 2	e, ex	2, 5
J11111083−7641574	ESO Hα 569	K7:, M2.5	1, 2	e, A_V, ex	11, 12
J11115400−7619311	CHXR 49NE	M1, K7−M0, M2.5	17, 11, 2	Li	4
J11142906−7625399[d]	ESO Hα 571	M5.5, M4.75	1, 2	NaK	7
J11152180−7724042[d]	ESO Hα 572	M5.5, M4.75	1, 2	NaK	7
J11160287−7624533	ESO Hα 574	K:, K7−M0	1, 2	e	10

[a] From the 2MASS Point Source Catalog.
[b] Uncertainties for classifications from this work are ±0.25 subclass unless noted otherwise.
[c] Membership in Chamaeleon I is indicated by $A_V \gtrsim 1$ and a position above the main sequence for the distance of Chamaeleon I ("A_V"), strong emission lines ("e"), Na I and K I strengths intermediate between those of dwarfs and giants ("NaK"), IR excess emission ("ex"), the shape of the gravity-sensitive steam bands ("H_2O"), strong Li absorption ("Li"), or a radial velocity that is similar to that of the known members of Chamaeleon I ("rv").
[d] Selected for spectroscopy because it appeared as a candidate member in Fig. 2.
[e] Separation of 1.1″ and position angle of 19° relative to T39A.

REFERENCES.—(1) Comerón et al. 2004; (2) this work; (3) Appenzeller 1979; (4) Rydgren 1980; (5) Appenzeller et al. 1983; (6) Gauvin & Strom 1992; (7) Gómez & Mardones 2003; (8) Brandner & Zinnecker 1997; (9) Comerón et al. 1999; (10) Feigelson & Kriss 1989; (11) Huenemoerder et al. 1994; (12) Alcalá et al. 1995; (13) Covino et al. 1997; (14) Saffe et al. 2003; (15) Luhman 2004a; (16) Luhman et al. 2004; (17) Hartigan 1993.

are not in the 2MASS Point Source Catalog, I have assigned new coordinate-based names. Additional names for the previously known members have been compiled by Carpenter et al. (2002) and Luhman (2004a). All spectral types in Table 3 are from this work. The spectra of the X-ray-selected targets were described by Feigelson & Lawson (2004). Comments on the classifications of other individual sources are provided in Appendix A.

The optical and IR spectra of the new and previously known members of Chamaeleon I in my spectroscopic sample are shown in Figures 7–9. The source 2M J1106−7732 is excluded because Luhman (2004b) already presented its spectrum, and C1-25 is not shown because its spectrum has a very low signal-to-noise ratio. Some of the spectra obtained with IMACS exhibit gaps in wavelength coverage that are produced by the boundaries between adjacent CCDs.

2.4. *Completeness of Census*

In § 4, I construct IMFs for a $1.5^\circ \times 0.35^\circ$ field encompassing most of the Chamaeleon I cloud (Fig. 1*a*) and the $0.22^\circ \times 0.28^\circ$ field in the southern subcluster that was imaged with ACS (Fig. 1*d*). To ensure that these IMFs are accurate representations of the stellar population in Chamaeleon I, in this section I evaluate the completeness of the current census of known members within these two fields as a function of mass and extinction. I also perform a completeness analysis for the substellar members within 3° of the center of Chamaeleon I, the results of which are used in § 5 to measure the large-scale spatial distribution of brown dwarfs.

I first consider the $1.5^\circ \times 0.35^\circ$ field. In Figure 10, I show the diagram of $J - H$ versus H from 2MASS for this area. The completeness limits of the 2MASS photometry are taken to be the magnitudes at which the logarithm of the number of sources as a function of magnitude departs from a linear slope and begins to turn over. In Figure 10, I have plotted the 10 Myr isochrone from Baraffe et al. (1998) for $A_J = 0$ and 1.2. I selected this isochrone because most members of Chamaeleon I fall above it on the Hertzsprung-Russell (H-R) diagram (§ 3). A comparison of the 2MASS completeness limits to the isochrones indicates that the photometric data should be complete for members with $M/M_\odot \geq 0.03$ (≲M8) and $A_J \leq 1.2$, with the exception

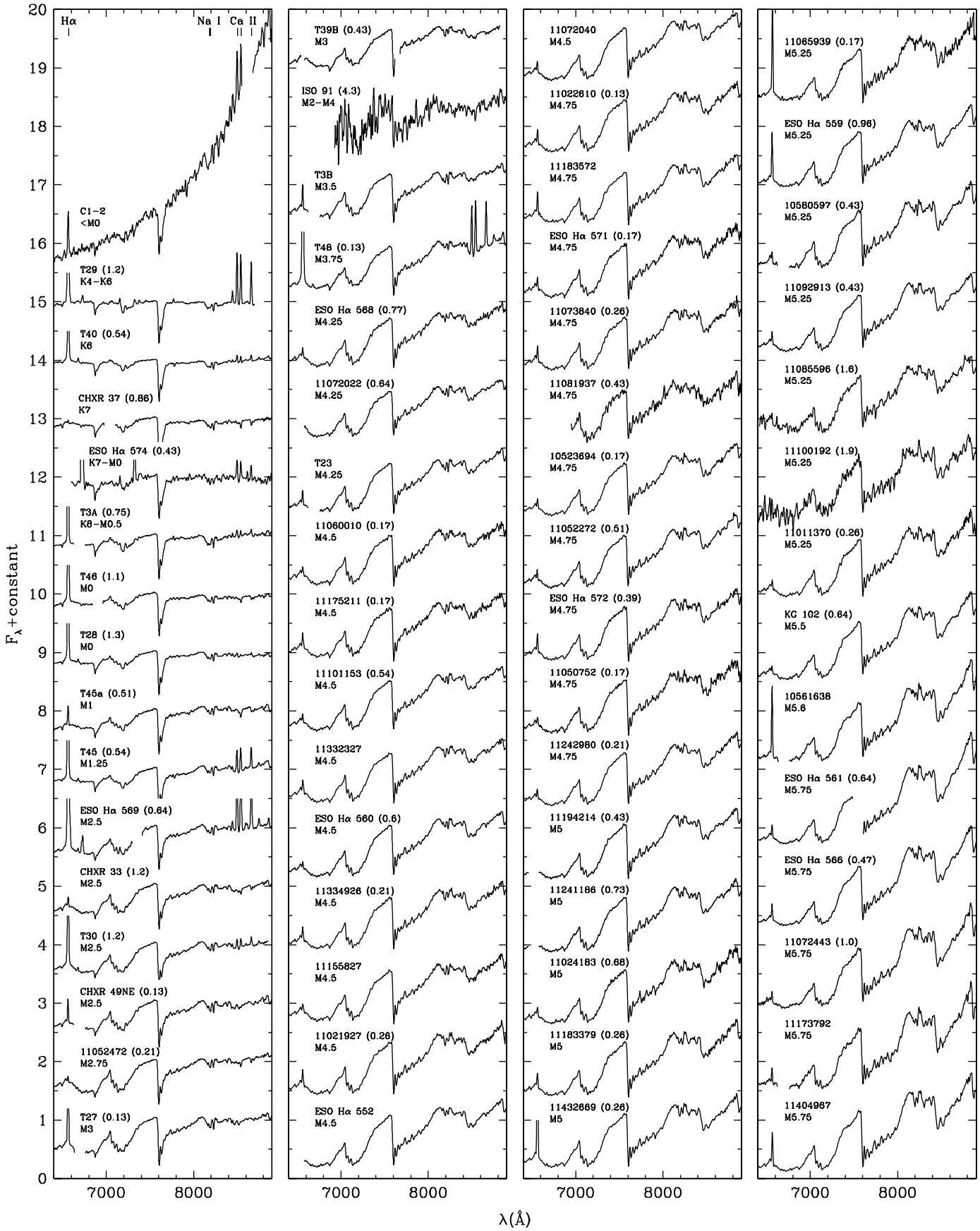


FIG. 7.— Optical spectra of previously known members of Chamaeleon I and new members identified in this work. With the exception of C1-2, the spectra have been corrected for extinction, which is quantified in parentheses by the magnitude difference of the reddening between 0.6 and 0.9 μm [$E(0.6-0.9)$]. The data are displayed at a resolution of 13 Å and are normalized at 7500 Å.

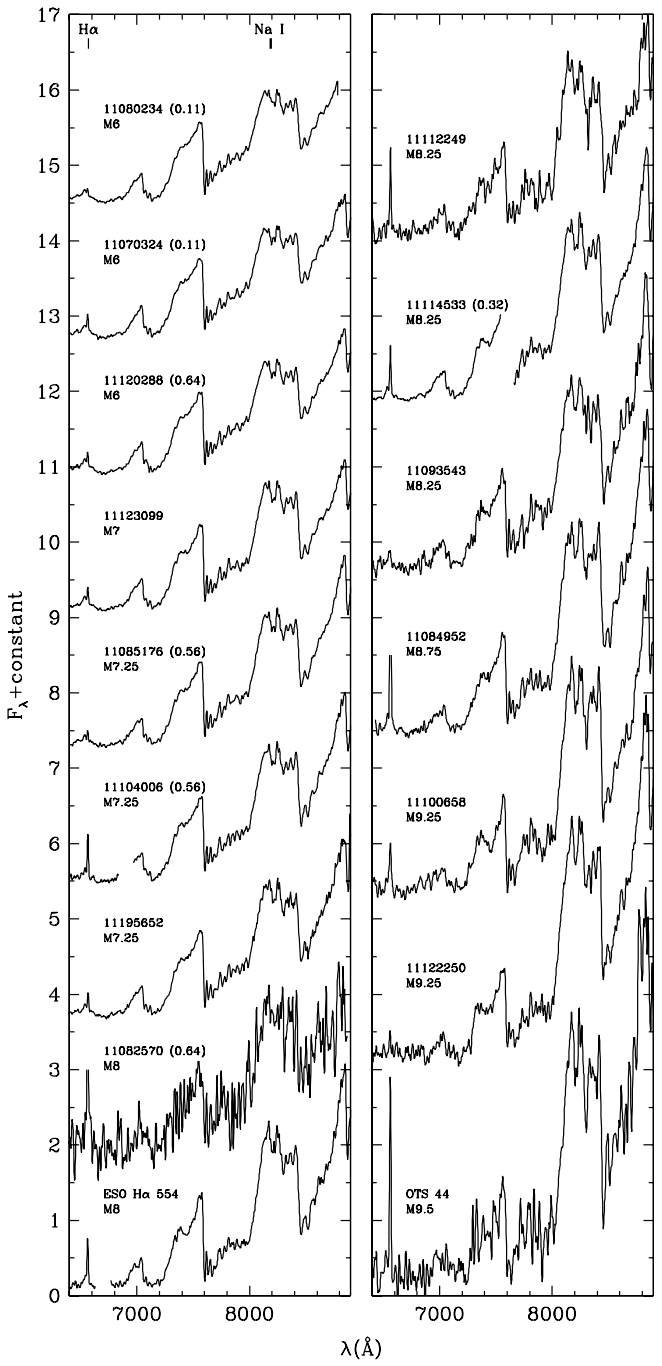


FIG. 8.—More optical spectra of previously known and new members of Chamaeleon I (see Fig. 7).

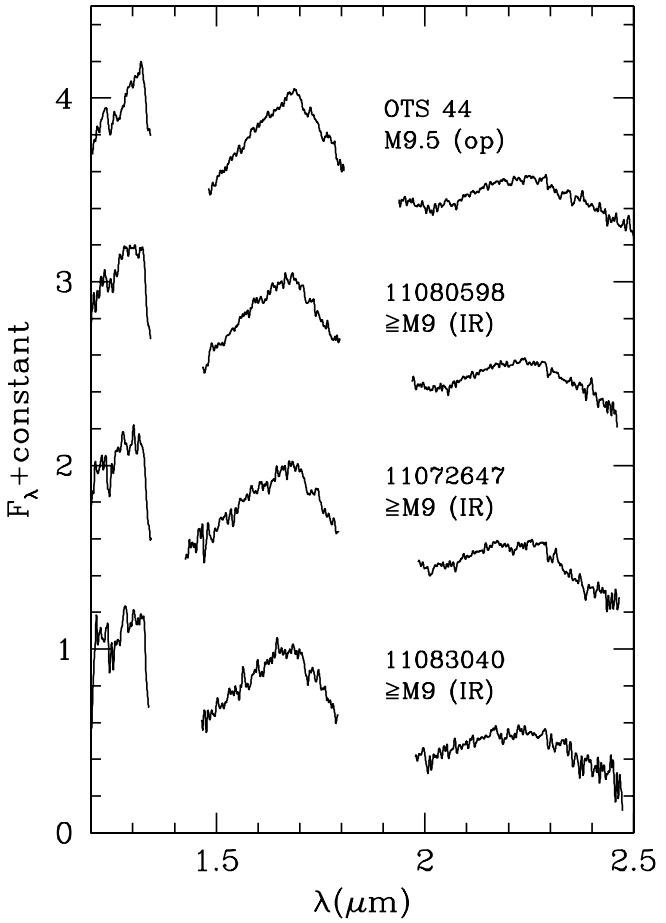


FIG. 9.—Near-IR spectra of the three new members of Chamaeleon I from Figs. 5 and 6 (*eight-digit identifications*) and a previously known member, OTS 44. The former are labeled with the spectra types derived from this comparison to OTS 44, which has an optical type of M9.5 (Fig. 8), and other optically classified late-type members. The spectra are displayed at a resolution of $R = 500$, are normalized at 1.68 μm, and are dereddened (§ 2.3).

of close companions and objects that are simultaneously near $M/M_{\odot} \sim 0.03$, $A_J \sim 1.2$, and $\tau \sim 10$ Myr. I have omitted in Figure 10 the 2MASS sources that are nonmembers according to spectroscopy or that are likely to be field stars because they are below the sequences of known members in Figures 2 and 4. The remaining sources either have been confirmed as members or lack sufficient data for the assessment of their membership. Based on these data, the current census in the $1.5^{\circ} \times 0.35^{\circ}$ field should be nearly 100% complete for $M/M_{\odot} \geq 0.03$ and $A_J \leq 1.2$. These completeness limits do not apply to objects that are seen in scattered light (e.g., edge-on disks) because they often appear below cluster sequences on color-magnitude diagrams and thus can be mistaken for field stars.

My ISPI near-IR images of Chamaeleon I encompassed the entire $0.22^{\circ} \times 0.28^{\circ}$ ACS field and are deeper than 2MASS. Therefore, for this field I have constructed the diagram of $J - H$ versus H in Figure 11 from a combination of 2MASS and ISPI photometry. For sources that are present in both sets of data, I adopt the measurement from ISPI if the photometric uncertainty from 2MASS is larger than 0.05 mag. The completeness limit of the ISPI data is estimated in the same manner as for 2MASS earlier in this section. As with Figure 10, I show the 10 Myr isochrone from Baraffe et al. (1998) except for a higher extinction of $A_J = 1.4$ and a lower minimum mass of 0.015 $M_{\odot}$. Sources that are likely to be nonmembers based on spectroscopy or their positions in Figures 2, 4, and 5 are omitted from Figure 11. I also reject sources that are resolved as galaxies in the ACS images. The remaining IR sources consist of confirmed members and sources with undetermined membership. A comparison of these two populations to the reddened isochrone and the ISPI completeness limit demonstrates that the current census of members within the ACS field is complete for $M/M_{\odot} \geq 0.01$ and $A_J \leq 1.4$.

Finally, I evaluate the completeness of the current census of brown dwarfs for the area outside of the $1.5^{\circ} \times 0.35^{\circ}$ field and within a radius of 3° from the center of Chamaeleon I. I consider only the regions that are covered by the Second DENIS Release, which are indicated in Figure 1. The diagram of $J - H$ versus H from 2MASS for this area is shown in Figure 12. I have excluded

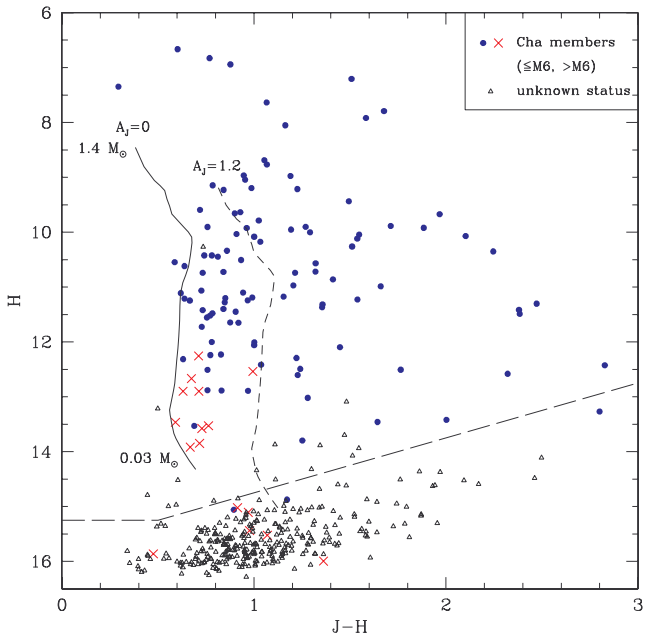


FIG. 10.—$J - H$ vs. H from 2MASS for the $1.5^\circ \times 0.35^\circ$ field in Fig. 1*a*. I have omitted the stars classified as nonmembers through spectroscopy (Table 4), as well as objects that are probable field stars because they are below the sequences of known members in Figs. 2 and 4. This diagram shows the remaining stars, which consist of known members of Chamaeleon I (*filled circles and crosses*) and stars whose membership is undetermined (*triangles*). The 10 Myr isochrone (1.4–0.03 $M_\odot$) from the evolutionary models of Baraffe et al. (1998) is shown for $A_J = 0$ (*solid line*) and $A_J = 1.2$ (*short-dashed line*). These measurements have completeness limits of $J = 15.75$ and $H = 15.25$ (*long-dashed line*).

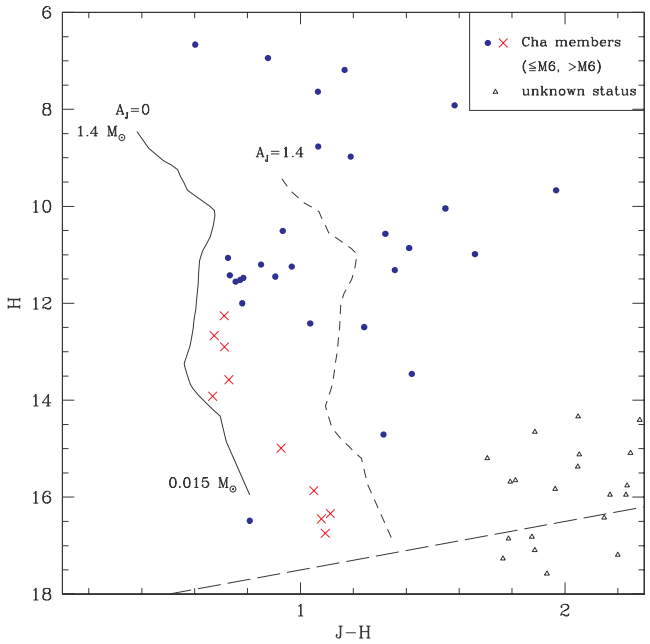


FIG. 11.—$J - H$ vs. H from 2MASS and ISPI for the $0.22^\circ \times 0.28^\circ$ field imaged with ACS in Fig. 1*d*. I have omitted the stars classified as nonmembers through spectroscopy (Table 4), objects that are probable field stars because they are below the sequences of known members in Figs. 2, 4, and 5, and sources that are resolved as galaxies in the ACS images. This diagram shows the remaining stars, which consist of known members of Chamaeleon I (*filled circles and crosses*) and stars whose membership is undetermined (*triangles*). The 10 Myr isochrone (1.4–0.015 $M_\odot$) from the evolutionary models of Baraffe et al. (1998) is shown for $A_J = 0$ (*solid line*) and $A_J = 1.4$ (*short-dashed line*). The measurements have completeness limits of $J = 18.5$ and $H = 18.25$ (*long-dashed line*).

2MASS sources that have been spectroscopically classified as nonmembers or that are likely to be field stars because they are below the sequences of known members in Figures 2 and 3. Because I am examining the completeness of only brown dwarfs in Chamaeleon I and not stellar members for the area in question, I have also omitted 2MASS sources whose colors are too blue for brown dwarfs; nearly all known members of Chamaeleon I with spectral types later than M6 have $i - K_s > 3$ and $H - K_s > 0.35$, so I have applied these thresholds. The resulting color-magnitude diagram in Figure 12 contains known members and sources whose membership is undetermined. Because most of the area considered here is outside of the Chamaeleon I dark clouds, the known members within it exhibit little extinction ($A_J < 0.6$), and the same is expected for any undiscovered members. For these low levels of extinction, Figure 12 indicates that the current census of Chamaeleon I is complete for $M/M_\odot \geq 0.03$ ($\lesssim$M8) out to a radius of 3° for the area covered by DENIS and outside of the central $1.5^\circ \times 0.35^\circ$ field.

2.5. *Summary of Updated Census*

It is useful to describe the statistics of the updated census of Chamaeleon I that includes the new members found in this work. The census presented by Luhman (2004a) consisted of 158 members, eight of which were later than M6. SGR 1 was included in that list of members, but I now classify it as a field star (Appendix A) and remove it from the census. During the time since Luhman (2004a) 16 members have been identified by Luhman (2004b), Luhman et al. (2004, 2005c, 2006), and Comerón et al. (2004). I also add ESO Hα 281 from Brandner & Zinnecker (1997), which was overlooked by Luhman (2004a). T3B and T39B were previously believed to be companions but were not counted as members by Luhman (2004a) because they lacked spectroscopic confirmation. Based on my spectral classifications of T3B and T39B, I include them in the census of members. When the 50 new members from this work are included, the latest census of Chamaeleon I contains 226 known members, 28 of which are later than M6.[2]

3. STAR FORMATION HISTORY

3.1. *H-R Diagram*

To place the members of Chamaeleon I on the H-R diagram, I first estimate their extinctions, effective temperatures, and bolometric luminosities. I exclude from this analysis 11 of the 226 known members whose spectral types are too uncertain for such estimates. When constructing an H-R diagram from an earlier census of Chamaeleon I, Luhman (2004a) adopted the average of the extinctions estimated from optical spectra and near-IR colors when both were available. I use a different approach in this work, adopting only the spectroscopically measured extinctions when possible. Following Luhman (2004a), the reddenings of the optical spectra are quantified by the color excess between 0.6 and 0.9 μm, which is denoted as $E(0.6 - 0.9)$ in Figures 7 and 8. These excesses are converted to A_J with the relation $A_J = E(0.6 - 0.9)/0.95$ (Luhman 2004a). Extinction estimates from spectra are available for 198 members (§ 2; Luhman 2004a, 2004b; Luhman et al. 2004, 2006). For the remaining 17 stars, I estimate extinctions from $J - H$ and $H - K_s$ in the manner described by Luhman (2004a).

[2] The number of objects in a given range of spectral types depends on the measurements that are adopted. I am adopting spectral types from this work, Luhman (2004a, 2004b), and Luhman et al. (2004, 2005c, 2006).

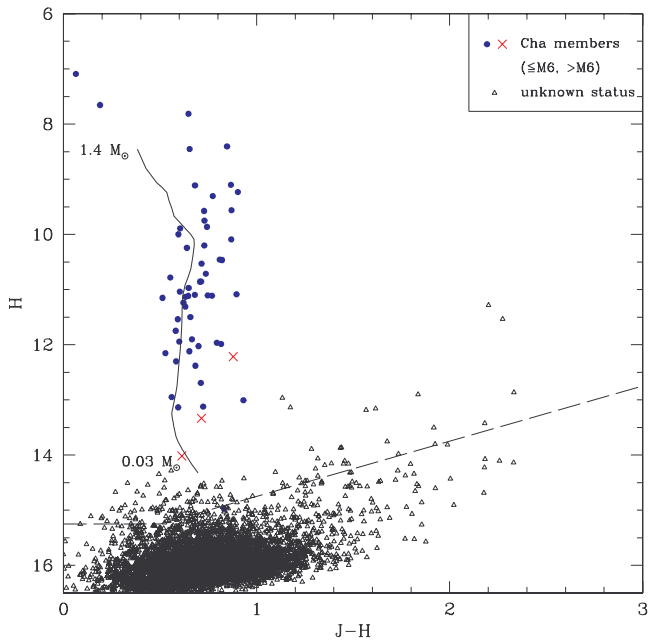


FIG. 12.—The $J - H$ vs. H from 2MASS for the area outside of the $1.5^\circ \times 0.35^\circ$ field in Fig. 1*a* and within a radius of 3° from the center of Chamaeleon I for which data are available from the Second DENIS Release (see Fig. 1*b*). I have omitted the stars classified as nonmembers through spectroscopy (Table 4), as well as objects that are probable field stars because they are below the sequences of known members in Figs. 2 and 3. I have also excluded ones with colors too blue to be substellar members of the cluster ($i - K_s < 3, H - K_s < 0.35$), with the exception of known members. The remaining sources shown in this diagram consist of known members of Chamaeleon I (*filled circles and crosses*) and stars whose membership is undetermined (*triangles*). The 10 Myr isochrone ($1.4–0.03\ M_\odot$) from the evolutionary models of Baraffe et al. (1998) is shown with no extinction (*solid line*). These measurements have completeness limits of $J = 15.75$ and $H = 15.25$ (*dashed line*).

The uncertainties of the extinctions estimated from spectroscopy are determined by the errors in relative flux calibration of the spectra. All of the targets observed with long-slit spectroscopy were observed with the slit aligned at the parallactic angle, which prevents errors in relative flux calibration due to atmospheric differential refraction (Filippenko 1982). On the other hand, the multislit observations generally were not performed at the parallactic angle because a given slit mask required a specific position angle. To ensure accurate relative flux calibration, I included slits in each mask for known members that have been previously observed with long-slit spectroscopy. I then compared the spectral slopes of the multislit and long-slit data to check the accuracy of the former. This analysis indicates errors in the relative flux calibration of the multislit data that correspond to $A_J \sim 0.13$.

Spectral types are converted to effective temperatures and bolometric luminosities are derived from *J*-band magnitudes with the same temperature scale and bolometric corrections used by Luhman (2004a), except that I adopt the *J*-band bolometric corrections from Dahn et al. (2002) for spectral types of M6 and later. For computing the luminosities, I adopt a distance modulus of 6.05 (Luhman 2007), which differs slightly from the value of 6.13 used in Luhman (2004a). For most members of Chamaeleon I, I used *J*-band measurements from 2MASS or my ISPI images. However, T39B, 2MASS 11072022−7738111, ESO Hα 281, T3B, T33B, and CHXR 73B are blended with brighter stars in those data. I estimate near-IR magnitudes for the first four sources by applying the differential photometry from Chelli et al. (1995) and Correia et al. (2006) to the 2MASS data. For T33A/B and CHXR 73B, I adopt the resolved photometry from Haisch et al. (2004) and Luhman et al. (2006), respectively. The typical uncertainties in A_J, J, and BC_J ($\sigma \sim 0.13$, 0.03, 0.1, respectively) correspond to errors of ± 0.07 in the relative values of $\log L_{\mathrm{bol}}$. When an uncertainty in the distance modulus is included ($\sigma \sim 0.13$), the total uncertainties are ± 0.08.

The extinctions, effective temperatures, bolometric luminosities, and adopted spectral types for the 215 known members of Chamaeleon I with spectral classifications are listed in Table 6. These temperatures and luminosities are plotted in Figure 13 for members later than G5. Separate H-R diagrams are shown for the members north and south of $\delta = -77^\circ$, which is the approximate midpoint between the northern and southern subclusters. The H-R diagram for types earlier than G5 is the same as that in Luhman (2004a) except for a small offset in luminosities because of the different adopted distances.

3.2. *Distribution of Ages*

In the H-R diagram for Chamaeleon I from Luhman (2004a) the sequence for Chamaeleon I closely resembled that of IC 348 in terms of age, with both clusters exhibiting median ages of $\sim$2 Myr with the models of Baraffe et al. (1998) and Chabrier et al. (2000). The same result is produced by the updated data shown in Figure 13. Because the census of Chamaeleon I is now larger and more complete, I can compare the ages of the northern and southern subclusters. In Figure 13, the northern sequence appears to be slightly fainter, and hence older, than the southern one. To better illustrate this age difference, I compare the distributions of model ages for the two subclusters in Figure 14. For masses of 0.1 to 1 $M_\odot$, the northern and southern subclusters have median ages of 2.8 and 2.5 Myr, respectively. For masses below 0.1 $M_\odot$, each sequence in Chamaeleon I becomes somewhat older on the model isochrones. Rather than a true variation of age with mass, this feature may be caused by an error in the adopted temperature scale or evolutionary models.

To interpret the distributions of isochronal ages in Figure 14 in terms of star formation histories, I must account for the observational errors in the age estimates. To do this, I assume that the errors follow Gaussian distributions. I adopt $\sigma = 0.13$, 0.1, and 0.1 mag to represent the errors from extinction (A_J), variability, and bolometric corrections, respectively. The sum of these errors in quadrature corresponds to $\sigma(\log L) = 0.08$, which is approximately equivalent to $\sigma(\log t) = 0.12$ (Hartmann 2001). Because the depth of Chamaeleon I should be only a few parsecs, the uncertainties in relative distances should have a negligible effect on the spread in luminosities. I also account for binaries in the manner described by Hartmann (2001), except that I assume an unresolved binary fraction of 30%, which should be a reasonable value for a sample like the one in Chamaeleon I that is dominated by low-mass stars (Reid & Gizis 1997).

I now convolve the error distributions with model star formation histories and compare the results to the distributions of isochronal ages in Figure 14. I consider two types of star formation histories, an instantaneous burst and an extended period of constant star formation. For the burst, I select an age that reproduces the median of the isochronal ages in Chamaeleon I. As shown in Figure 14, a burst at 3 Myr closely resembles the age distribution of the southern sample at ages beyond 1 Myr. The agreement in the widths of the observed and model distributions suggests that the combined observational errors are not significantly larger than the adopted value of $\sigma(\log t) = 0.12$. On the other hand, the northern sample exhibits a distribution of ages that is broader than the model distribution for a single burst. If the observational errors are similar between the two halves of Chamaeleon I, then the broader age distribution in the north indicates the presence of

TABLE 6

DERIVED PROPERTIES FOR MEMBERS OF CHAMAELEON I

2MASS[a]	Name	Adopted Spectral Type	$T_{\rm eff}$[b] (K)	A_J	$L_{\rm bol}$ ($L_\odot$)	IMF[c]
J10463795−7736035	HD 93828	F0	7200	0.00	8.9	...
J10523694−7440287	...	M4.75	3161	0.18	0.10	...
J10550964−7730540	ESO Hα 552	M4.5	3198	0.34	0.083	...
...	T3B	M3.5	3342	0.00	0.040	...
J10555973−7724399	T3A	M0	3850	0.79	0.42	...
J10561638−7630530	ESO Hα 553	M5.6	3044	0.00	0.031	...
J10563044−7711393	T4	M0.5	3778	0.23	0.57	...
J10574219−7659356	T5	M3.25	3379	0.34	0.33	...
J10580597−7711501	...	M5.25	3091	0.45	0.022	...
J10581677−7717170	T6	K0	5250	0.42	1.9	...
J10590108−7722407	T7	K8	3955	0.34	0.57	...
J10590699−7701404	T8	K2	4900	0.00	2.4	...
J11004022−7619280	T10	M3.75	3306	0.20	0.077	...
J11011370−7722387	...	M5.25	3091	0.27	0.025	...
J11011875−7627025	CHXR 9C	M2.25	3524	0.45	0.56	...
J11011926−7732383	...	M7.25	2838	0.45	0.021	...
...	Cha J11011944−7732374	M8.25	2632	0.00	0.0065	...
J11013205−7718249	ESO Hα 554	M8	2710	0.00	0.0046	...
J11021927−7536576	...	M4.5	3198	0.27	0.062	...
J11022491−7733357	T11	K6	4205	0.07	1.2	...
J11022610−7502407	...	M4.75	3161	0.14	0.075	...
J11023265−7729129	CHXR 71	M3	3415	0.47	0.17	...
J11024183−7724245	[LM04] 423	M5	3125	0.72	0.049	...
J11025504−7721508	T12	M4.5	3198	0.00	0.081	...
J11034186−7726520	ISO 28	M5.5	3058	0.61	0.036	...
J11034764−7719563	Hn 2	M5	3125	0.68	0.18	...
J11035682−7721329	CHXR 12	M3.5	3342	0.20	0.21	...
J11040425−7639328	CHSM 1715	M4.25	3234	0.74	0.045	...
J11040909−7627193	T14	K5	4350	0.45	0.95	...
J11041060−7612490	CHSM 1982	M6	2990	0.11	0.019	...
J11042275−7718080	T14A	K7	4060	0.45	0.013	...
J11044258−7741571	ISO 52	M4	3270	0.36	0.093	...
J11045100−7625240	CHXR 14N	K8	3955	0.23	0.35	...
J11045285−7625514	CHXR 14S	M1.75	3596	0.23	0.26	...
J11045701−7715569	T16	M3	3415	1.60	0.21	...
J11050752−7812063	...	M4.75	3161	0.18	0.077	...
J11051467−7711290	Hn 4	M3.25	3379	0.79	0.31	1
J11052272−7709290	...	M4.75	3161	0.54	0.035	1
J11052472−7626209	...	M2.75	3451	0.23	0.12	1
J11054300−7726517	CHXR 15	M5.25	3091	0.11	0.11	1
J11055261−7618255	T20	M1.5	3632	0.11	0.35	1
J11055780−7607488	HD 96675	B6.5	13500	0.02	98	...
J11060010−7507252	...	M4.5	3198	0.18	0.047	...
J11061540−7721567	T21	G5	5770	0.92	16	1
J11061545−7737501	Cam 2-19	M2.75	3451	2.82	0.44	...
J11062554−7633418	ESO Hα 559	M5.25	3091	1.01	0.052	1
...	CHXR 73B	$\geq$M9	$\leq$2400	2.12	0.0017	...
J11062877−7737331	CHXR 73A	M3.25	3379	1.85	0.17	...
J11063276−7625210	CHSM 7869	M6	2990	0.45	0.0098	1
J11063799−7743090	Cha Hα 12	M6.5	2935	0.18	0.024	1, 2
J11063945−7736052	ISO 79	M5.25	3091	0.77	0.0074	1, 2
J11064180−7635489	Hn 5	M4.5	3198	0.32	0.11	1
J11064346−7726343	T22	M3	3415	0.99	0.42	1
J11064510−7727023	CHXR 20	K6	4205	1.08	1.1	1
J11065733−7742106	CHXR 74	M4.25	3234	0.54	0.15	1,2
J11065906−7718535	T23	M4.25	3234	0.00	0.11	1
J11065939−7530559	...	M5.25	3091	0.18	0.012	...
J11070324−7610565	...	M6	2990	0.11	0.010	...
...	ESO Hα 281	M4.5	3198	1.05	0.057	1
J11070925−7718471	ISO 91	M3	3415	4.51	0.25	...
J11071148−7746394	CHXR 21	M3	3415	1.04	0.34	1
J11071181−7625501	CHSM 9484	M5.25	3091	0.50	0.018	1
J11071206−7632232	T24	M0.5	3778	0.63	0.36	1
J11071330−7743498	CHXR 22E	M3.5	3342	1.35	0.22	2
J11071668−7735532	Cha Hα 1	M7.75	2752	0.00	0.015	1, 2

TABLE 6—*Continued*

2MASS[a]	Name	Adopted Spectral Type	$T_{\rm eff}$[b] (K)	A_J	$L_{\rm bol}$ ($L_\odot$)	IMF[c]
J11071860−7732516	Cha Hα 9	M5.5	3058	1.62	0.046	...
J11071915−7603048	T25	M2.5	3488	0.45	0.24	...
J11072022−7738111	...	M4.25	3234	0.68	0.16	1, 2
J11072040−7729403	ISO 99	M4.5	3198	0.00	0.12	1
J11072074−7738073	T26	G2	5860	0.75	12	1, 2
J11072443−7743489	[LM04] 429	M5.75	3024	1.08	0.036	1, 2
...	Cha J11072647−7742408	≥M9	≤2400	0.28	0.00043	1, 2
J11072825−7652118	T27	M3	3415	0.14	0.22	1
J11073519−7734493	CHXR 76	M4.25	3234	0.68	0.091	1
J11073686−7733335	CHXR 26	M3.5	3342	2.26	0.66	...
J11073775−7735308	Cha Hα 7	M7.75	2752	0.23	0.014	1, 2
J11073832−7747168	ESO Hα 560	M4.5	3198	0.63	0.078	1
J11073840−7552519	...	M4.75	3161	0.27	0.034	...
J11074245−7733593	Cha Hα 2	M5.25	3091	1.06	0.11	1, 2
J11074366−7739411	T28	M0	3850	1.35	1.4	2
J11074610−7740089	Cha Hα 8	M5.75	3024	0.45	0.037	1, 2
J11074656−7615174	CHSM 10862	M5.75	3024	0.45	0.013	...
J11075225−7736569	Cha Hα 3	M5.5	3058	0.63	0.070	1, 2
J11075588−7727257	CHXR 28	K6	4205	1.54	4.0	...
J11075730−7717262	CHXR 30B	M1.25	3669	3.16	0.22	...
J11075792−7738449	T29	K6	4205	1.24	2.4	2
J11075809−7742413	T30	M2.5	3488	1.26	0.15	2
J11075993−7715317	ESO Hα 561	M5.75	3024	0.68	0.058	1
J11080002−7717304	CHXR 30A	K8	3955	2.98	1.4	...
J11080148−7742288	T31	K8	3955	0.72	3.0	1, 2
J11080234−7640343	[LM04] 717	M6	2990	0.11	0.023	1
J11080297−7738425	ISO 126	M1.25	3669	1.35	0.33	2
J11080329−7739174	T32	B9.5	10010	0.72	70	1, 2
J11080609−7739406	...	≥M9	≤2400	0.00	0.00059	1, 2
...	T33B	K6	4205	0.52	0.78	1, 2
J11081509−7733531	T33A	G7	5630	0.85	2.8	1, 2
J11081648−7744371	T34	M3.75	3306	0.29	0.15	1
J11081703−7744118	Cha Hα 13	M5.5	3058	0.32	0.083	1, 2
J11081850−7730408	ISO 138	M6.5	2935	0.00	0.0075	1
J11081896−7739170	Cha Hα 4	M5.5	3058	0.23	0.055	1, 2
...	Cha J11081938−7731522	M4.75	3161	0.45	0.00062	...
J11082238−7730277	ISO 143	M5	3125	1.13	0.088	1
J11082404−7739299	Cha Hα 10	M6.25	2962	0.11	0.0066	1, 2
J11082410−7741473	Cha Hα 5	M5.5	3058	0.56	0.082	1, 2
J11082570−7716396	...	M8	2710	0.68	0.0014	1
J11082650−7715550	ISO 147	M5.75	3024	0.68	0.019	1
J11082927−7739198	Cha Hα 11	M7.25	2838	0.00	0.0047	1, 2
...	Cha J11083040−7731387	≥M9	≤2400	0.28	0.00033	1, 2
J11083905−7716042	T35	K8	3955	1.31	0.53	...
J11083952−7734166	Cha Hα 6	M5.75	3024	0.38	0.057	1, 2
J11084069−7636078	CHXR 33	M2.5	3488	1.26	0.74	...
J11084952−7638443	...	M8.75	2478	0.00	0.0014	1
J11085090−7625135	T37	M5.25	3091	0.11	0.038	1
J11085176−7632502	[LM04] 737	M7.25	2838	0.59	0.011	1
J11085421−7732115	CHXR 78C	M5.25	3091	0.56	0.066	1, 2
J11085464−7702129	T38	M0.5	3778	0.90	0.34	1
J11085497−7632410	ISO 165	M5.5	3058	0.63	0.035	1
J11085596−7727132	ISO 167	M5.25	3091	1.69	0.061	...
J11090512−7709580	Hn 7	M4.75	3161	0.18	0.068	1
...	T39A	M2	3560	0.34	0.33	1
...	T39B	M3	3415	0.45	0.26	...
...	Cha J11091363−7734446	≥M9	≤2400	0.28	0.00047	1, 2
J11091380−7628396	CHXR 35	M4.75	3161	0.18	0.072	1
J11091769−7627578	CHXR 37	K7	4060	0.90	1.1	1
J11091812−7630292	CHXR 79	M1.25	3669	1.92	0.55	...
J11092266−7634320	C1-6	M1.25	3669	3.27	0.80	...
J11092379−7623207	T40	K6	4205	0.56	0.53	1
J11092913−7659180	[LM04] 602	M5.25	3091	0.45	0.024	1
J11093543−7731390	...	M8.25	2632	0.00	0.0014	1, 2
J11093777−7710410	Cam 2-42	K7	4060	3.16	2.0	...
J11094006−7628391	CHXR 40	M1.25	3669	0.56	0.68	1

TABLE 6—*Continued*

2MASS[a]	Name	Adopted Spectral Type	$T_{\rm eff}$[b] (K)	A_J	$L_{\rm bol}$ ($L_\odot$)	IMF[c]
J11094260−7725578	C7-1	M5	3125	1.92	0.23	...
J11094525−7740332	ESO Hα 566	M5.75	3024	0.50	0.058	1, 2
J11094621−7634463	Hn 10E	M3.25	3379	1.01	0.15	1
J11094742−7726290	B43	M3.25	3379	2.26	0.22	...
J11094918−7731197	KG 102	M5.5	3058	0.68	0.036	1
J11095003−7636476	T41	B9	10500	0.70	57	1
J11095215−7639128	ISO 217	M6.25	2962	0.68	0.023	1
J11095262−7740348	CHSM 15991	M3	3415	0.79	0.0029	...
J11095336−7728365	ISO 220	M5.75	3024	1.71	0.030	...
J11095340−7634255	T42	K5	4350	1.47	3.0	...
J11095407−7629253	T43	M2	3560	1.47	0.48	...
J11095437−7631113	ISO 225	M1.75	3596	1.24	0.013	...
J11095873−7737088	T45	M1.25	3669	0.56	0.84	1, 2
J11100010−7634578	T44	K5	4350	1.35	5.5	...
J11100192−7725451	[LM04] 419	M5.25	3091	2.03	0.062	...
J11100369−7633291	Hn 11	K8	3955	2.14	0.66	...
J11100469−7635452	T45A	M1	3705	0.54	0.43	1
J11100658−7642486	...	M9.25	2350	0.00	0.0010	1
J11100704−7629376	T46	M0	3850	1.13	1.4	1
J11100785−7727480	ISO 235	M5.5	3058	2.41	0.11	...
J11100934−7632178	OTS 44	M9.5	2300	0.00	0.00077	1
J11101141−7635292	ISO 237	K5.5	4278	1.92	1.2	...
J11101153−7733521	...	M4.5	3198	0.56	0.077	1
J11102226−7625138	CHSM 17173	M8	2710	0.00	0.013	1
J11102852−7716596	Hn 12W	M5.5	3058	0.00	0.066	1
J11103481−7722053	[LM04] 405	M4	3270	1.94	0.32	...
J11103644−7722131	ISO 250	M4.75	3161	2.32	0.23	...
J11103801−7732399	CHXR 47	K3	4730	1.44	2.6	...
J11104006−7630547	...	M7.25	2838	0.59	0.0082	1
J11104141−7720480	ISO 252	M6	2990	0.97	0.022	1
J11104959−7717517	T47	M2	3560	1.17	0.42	1
J11105076−7718031	ESO Hα 568	M4.25	3234	0.81	0.11	1
J11105333−7634319	T48	M3.75	3306	0.14	0.13	1
J11105359−7725004	ISO 256	M4.5	3198	2.55	0.070	...
J11105597−7645325	Hn 13	M5.75	3024	0.23	0.13	1
J11111083−7641574	ESO Hα 569	M2.5	3488	0.68	0.0030	...
J11112249−7745427	[LM04] 436	M8.25	2632	0.00	0.0022	...
J11112260−7705538	ISO 274	M4.5	3198	0.45	0.10	...
J11113474−7636211	CHXR 48	M2.5	3488	0.23	0.21	...
J11113965−7620152	T49	M2	3560	0.34	0.37	...
J11114533−7636505	[LM04] 743	M8	2710	0.34	0.0033	...
J11114632−7620092	CHX 18N	K6	4205	0.20	1.3	...
J11115400−7619311	CHXR 49NE	M2.5	3488	0.14	0.36	...
J11120288−7722483	...	M6	2990	0.68	0.022	...
J11120327−7637034	CHXR 84	M5.5	3058	0.00	0.063	...
J11120351−7726009	ISO 282	M4.75	3161	1.01	0.030	...
J11120984−7634366	T50	M5	3125	0.11	0.15	...
J11122250−7714512	...	M9.25	2350	0.00	0.0015	...
J11122441−7637064	T51	K3.5	4660	0.00	1.0	...
J11122772−7644223	T52	G9	5410	0.42	5.0	...
J11123092−7644241	T53	M1	3705	0.79	0.39	...
J11123099−7653342	[LM04] 601	M7	2880	0.00	0.0074	...
J11124210−7658400	CHXR 54	M1	3705	0.34	0.41	...
J11124268−7722230	T54	G8	5520	0.60	4.2	...
J11124299−7637049	CHXR 55	K4.5	4470	0.31	0.61	...
J11124861−7647066	Hn 17	M4	3270	0.09	0.053	...
J11132012−7701044	CHXR 57	M2.75	3451	0.11	0.18	...
J11132446−7629227	Hn 18	M3.5	3342	0.14	0.073	...
J11132737−7634165	CHXR 59	M2.75	3451	0.11	0.24	...
J11132970−7629012	CHXR 60	M4.25	3234	0.09	0.089	...
J11133356−7635374	T55	M4.5	3198	0.07	0.080	...
J11141565−7627364	CHXR 62	M3.75	3306	0.38	0.15	...
J11142454−7733062	Hn 21W	M4	3270	0.72	0.11	...
J11142611−7733042	Hn 21E	M5.75	3024	0.56	0.042	...
J11142906−7625399	ESO Hα 571	M4.75	3161	0.18	0.037	...
J11145031−7733390	B53	M2.75	3451	0.00	0.24	...

TABLE 6—*Continued*

2MASS[a]	Name	Adopted Spectral Type	$T_{\rm eff}$[b] (K)	A_J	$L_{\rm bol}$ ($L_\odot$)	IMF[c]
J11152180−7724042	ESO Hα 572	M4.75	3161	0.41	0.096	...
J11155827−7729046	...	M4.5	3198	0.00	0.057	...
J11160287−7624533	ESO Hα 574	K8	3955	0.45	0.0034	...
J11173700−7704381	T56	M0.5	3778	0.16	0.39	...
J11173792−7646193	...	M5.75	3024	0.00	0.013	...
J11175211−7629392	...	M4.5	3198	0.18	0.087	...
J11181957−7622013	CHXR 68B	M2.25	3524	0.18	0.15	...
J11182024−7621576	CHXR 68A	K8	3955	0.23	0.70	...
J11183379−7643041	...	M5	3125	0.00	0.097	...
J11183572−7935548	...	M4.75	3161	0.00	0.21	...
J11194214−7623326	...	M5	3125	0.23	0.033	...
J11195652−7504529	...	M7.25	2838	0.00	0.0077	...
J11241186−7630425	...	M5	3125	0.77	0.047	...
J11242980−7554237	...	M4.75	3161	0.23	0.18	...
J11332327−7622092	...	M4.5	3198	0.00	0.20	...
J11334926−7618399	...	M4.5	3198	0.23	0.058	...
J11404967−7459394	...	M5.75	3024	0.00	0.027	...
J11432669−7804454	...	M5	3125	0.27	0.096	...

[a] From the 2MASS Point Source Catalog.
[b] Temperature scale from Luhman et al. (2003b).
[c] Indicates whether each object is included in the IMFs in Fig. 15 for the $1.5^\circ \times 0.35^\circ$ ("1") and $0.22^\circ \times 0.28^\circ$ ("2") fields in Fig. 1.

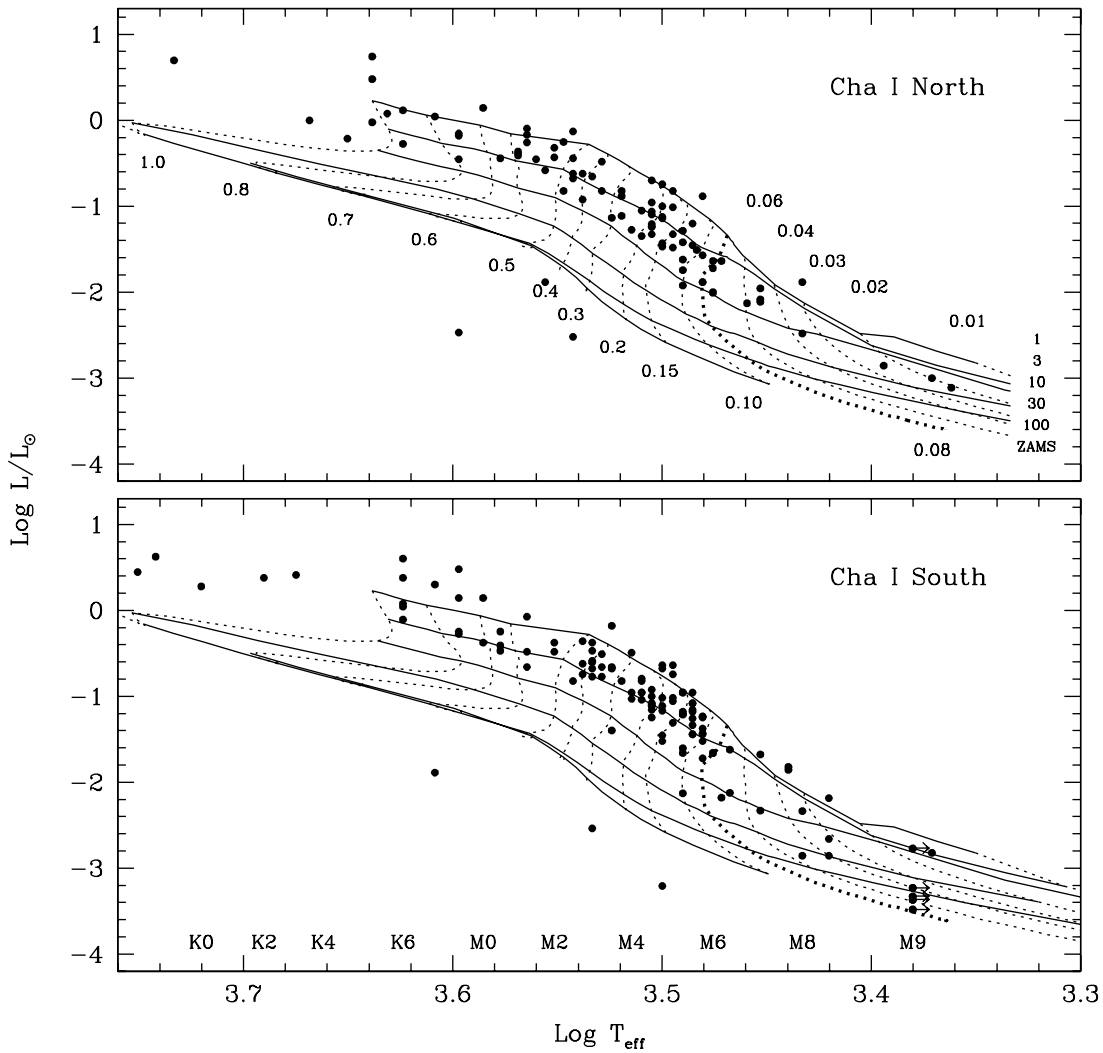


FIG. 13.—H-R diagrams for the northern (*top*, $\delta > -77^\circ$) and southern (*bottom*, $\delta < -77^\circ$) subclusters in Chamaeleon I. These data are shown with the theoretical evolutionary models of Baraffe et al. (1998) ($0.1 < M/M_\odot \leq 1$) and Chabrier et al. (2000) ($M/M_\odot \leq 0.1$), where the mass tracks (*dotted lines*) and isochrones (*solid lines*) are labeled in units of solar masses and megayears, respectively. The typical uncertainties are ±0.25 subclass and ±0.08 for spectral types and log $L_{\rm bol}$, respectively.

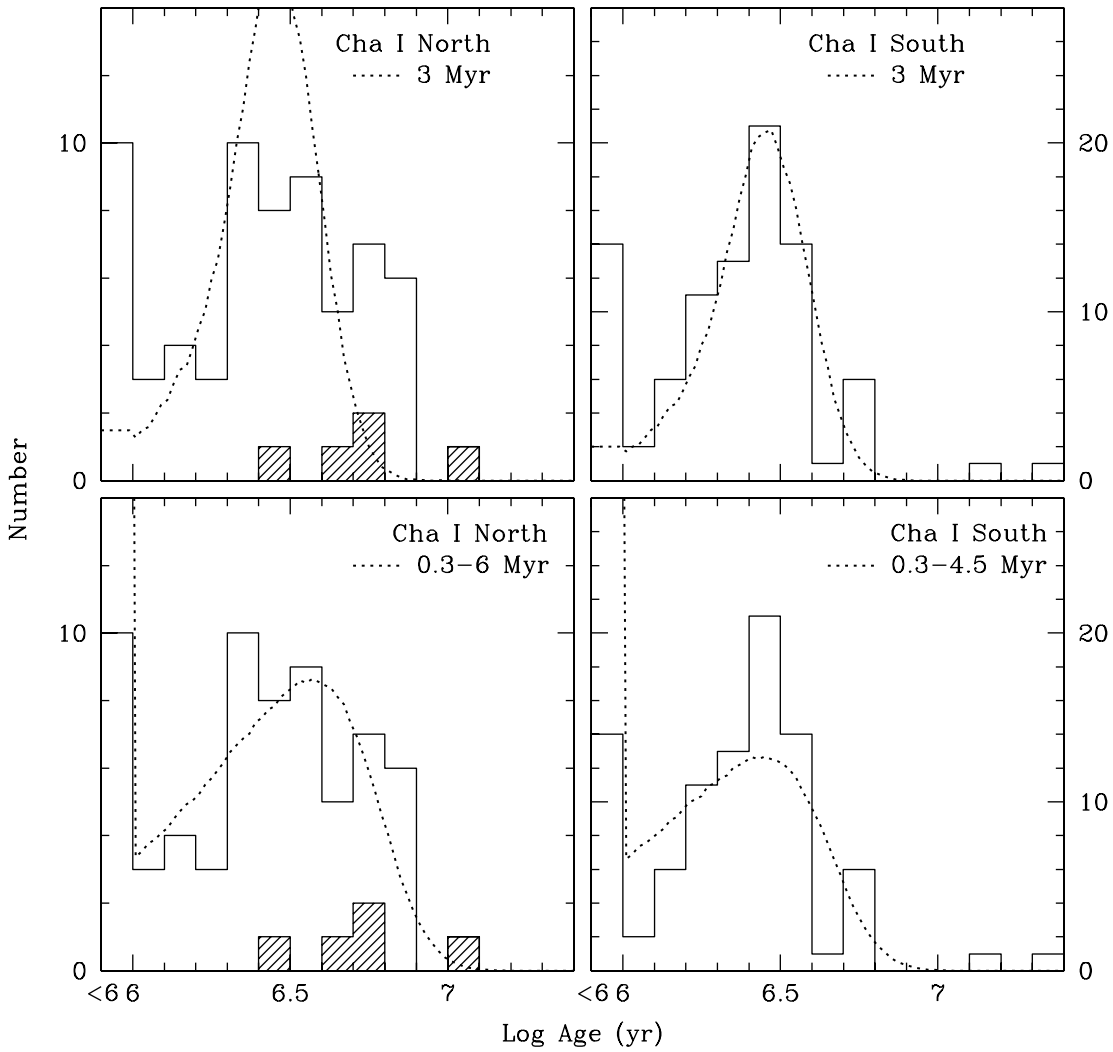


FIG. 14.—Distributions of isochronal ages from Fig. 13 for stars between 0.1 and 1 $M_{\odot}$ in the northern (*left*, $\delta > -77^{\circ}$) and southern (*right*, $\delta < -77^{\circ}$) subclusters in Chamaeleon I. For comparison, I show the distributions from a burst of star formation (*upper dotted lines*) and an extended period of constant star formation (*lower dotted lines*) convolved with the expected error distributions and normalized to the data at 1–10 Myr. The five young stars directly north of the Chamaeleon I clouds in Fig. 1*b* (*hatched histogram*, $\delta > -76^{\circ}$) appear to have older ages, on average, than the two subclusters.

a larger age spread and that star formation began 1–2 Myr earlier in the northern subcluster than in the southern one.

For both the northern and southern subclusters, the burst model produces too few stars with isochronal ages less than 1 Myr. Indeed, the presence of protostars in this region demonstrates that star formation is ongoing (Reipurth et al. 1996). Therefore, I also consider a constant star formation rate that extends to the present time. For comparison to the data in Figure 14, I select a lower limit of 0.3 Myr for the ages of stars in this model because most of the protostars lack spectral classifications and thus are absent from the H-R diagram in Figure 13. The same approach was used by Hartmann (2001) for Taurus. After varying the upper age limit for this model, I find that values of 6 and 4.5 Myr provide the best match to the data in the northern and southern samples, respectively, although they produce too many stars younger than 1 Myr. The models for a burst and periods of constant star formation bracket the data for the two subclusters, which suggests that star formation has occurred for the past 3–4 Myr in the south and 5–6 Myr in the north at rates that have declined with time. Thus, I do not find evidence in these data for Chamaeleon I to support the idea that star formation begins slowly and accelerates during the lifetime of a molecular cloud (Palla & Galli 1997; Palla & Stahler 1999, 2000, 2002).

In the preceding analysis, I have inferred ages for stars in Chamaeleon I with the model isochrones of Baraffe et al. (1998) and Chabrier et al. (2000). Use of other models would produce different age estimates. However, because the evolution of low-mass stars along Hayashi tracks approximately follows $\log t \propto \log L$ (Hartmann 1998), the distribution of $\log t$ is a reflection of the distribution of observed $\log L$ for any set of models. Thus, the shape of the distribution of isochronal ages shown in Figure 14 is insensitive to the choice of models, while the average age can vary by 0.1–0.2 in $\log t$ from one set of models to another because of differences in birth lines.

3.3. *Cloud Morphology*

The difference in isochronal ages between the northern and southern subclusters is consistent with the relative levels of obscuration toward their members. For instance, the fraction of stars residing outside of the extinction contours in Figure 1 is higher in the northern subcluster than in the southern one. The presence of a north-south age gradient is further supported by an examination of the string of five young stars directly north of the cloud at $\delta > -76^{\circ}$ that have been found in this work (see Fig. 1). The distribution of the isochronal ages of these stars is shown in Figure 14, which indicates that these stars are older, on average, than

the northern and southern samples. Based on these age data, I speculate that star formation in this region began in a small cloudlet north of the currently existing dark clouds, producing the B star HD 96675 and ~5–10 other stars, and propagated south to form the two larger subclusters. The apparent gradient in median age and cloud morphology between the northern and southern subclusters implies that the Chamaeleon I clouds are dissipating on a timescale of ~6 Myr after the initiation of star formation, which is consistent with previous estimates of molecular cloud lifetimes (Elmegreen 2000; Hartmann et al. 2001 and references therein).

According to theoretical evolutionary models (§ 4.2), the masses of the 215 members with spectral classifications range from ~0.01 to 3.5 $M_\odot$ and have a median value of 0.21 $M_\odot$. The combined mass of these objects is 86 $M_\odot$. After including the known members that lack measured spectral types, the total mass of the known stars and brown dwarfs in Chamaeleon I is ~100 $M_\odot$. Because most undiscovered members of the cluster are probably brown dwarfs, their inclusion would have a negligible effect on this estimate. The combination of the mass of the stellar population with a mass of ~1000 $M_\odot$ for the cloud (Boulanger et al. 1998; Mizuno et al. 2001) implies a star formation efficiency of ~10% for Chamaeleon I. This value is an upper limit because the cloud was probably more massive in the past.

4. INITIAL MASS FUNCTION

4.1. *Defining the Sample*

In this section, I measure IMFs for the $1.5^\circ \times 0.35^\circ$ and $0.22^\circ \times 0.28^\circ$ fields in Chamaeleon I that are indicated in Figure 1. Cluster members at higher masses can be detected through larger amounts of extinction. Therefore, to avoid IMF measurements that are biased in mass, I construct them from extinction-limited samples of known members. For the $1.5^\circ \times 0.35^\circ$ and $0.22^\circ \times 0.28^\circ$ fields, I select limits of $A_J \leq 1.2$ and ≤ 1.4, respectively. The current census of cluster members should be complete down to 0.03 and 0.01 $M_\odot$ for these areas and ranges of extinctions (§ 2.4). The extinctions used in creating these extinction-limited samples are those listed in Table 6 for the 215 members with spectral classifications. Eleven additional members lack extinction estimates because their spectral types are too uncertain, but they have very red near-IR colors that are indicative of extinctions well beyond the limits adopted for the two IMFs. Pairs of members with separations less than 2″ are treated as one source in the IMFs. In these cases, I adopt the masses of the earlier components. The six stars that appear below the main sequence in Figure 13 are rejected from the IMF samples because the census is not complete for subluminous objects of this kind. After applying these criteria to the census of Chamaeleon I, I arrive at IMF samples that contain 85 and 34 members for the $1.5^\circ \times 0.35^\circ$ and $0.22^\circ \times 0.28^\circ$ fields, respectively.

4.2. *Estimating Masses*

For the objects in the IMF samples, I estimate masses from their positions on the H-R diagram by using the theoretical evolutionary models of Baraffe et al. (1998) and Chabrier et al. (2000) for $M/M_\odot \leq 1$ and the models of Palla & Stahler (1999) for $M/M_\odot > 1$ because they provide the best agreement with observational constraints (Luhman et al. 2003b, 2005a; Luhman & Potter 2006). As noted in § 3, some of the late-type members of Chamaeleon I have rather old isochronal ages in Figure 13. For the purposes of this work, I assume that these old apparent ages are caused by errors in the luminosities, temperature scale, or models and that these objects in reality have the same ages as the stellar members. Therefore, for members later than M7 that are below the 10 Myr isochrone, I estimate masses from their spectral types assuming that they have ages of 1–3 Myr.

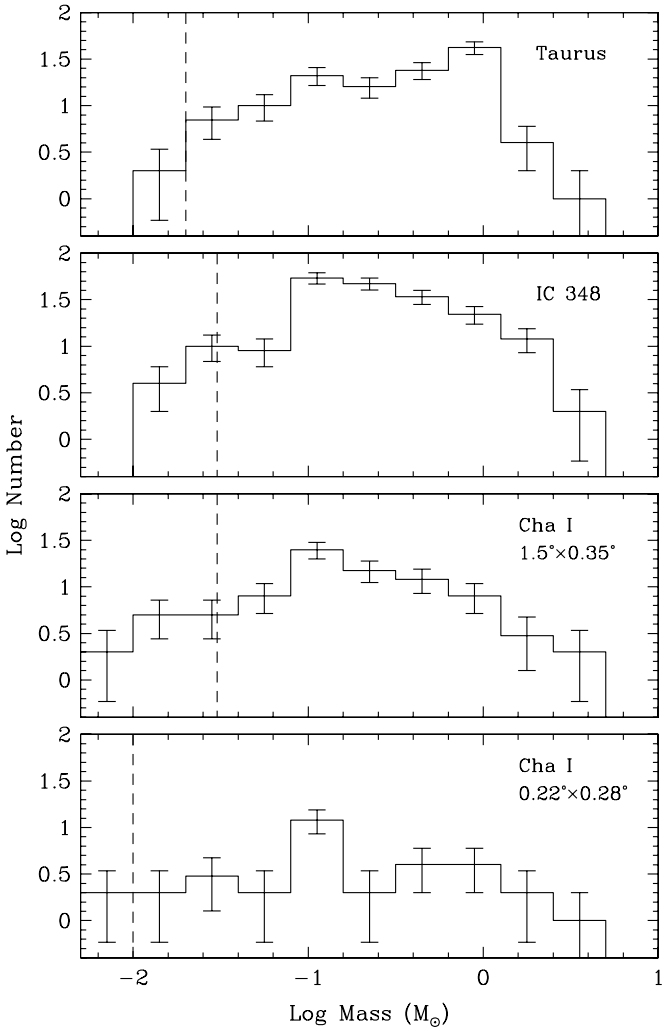


FIG. 15.—IMFs for extinction-limited samples in Taurus (Luhman 2004d), IC 348 (Luhman et al. 2003b), and the $1.5^\circ \times 0.35^\circ$ and $0.22^\circ \times 0.28^\circ$ fields in Chamaeleon I in Fig. 1. The completeness limits of these samples are indicated (*dashed lines*). In the units of this diagram, the Salpeter slope is 1.35.

I estimate the masses of the known members classified as ≥M9 by comparing their luminosities to the values predicted for the evolutionary models of Chabrier et al. (2000) and Burrows et al. (1997). To account for the large range of isochronal ages exhibited by the late-type members in Figure 13, I adopt a conservatively large range of ages of 1–30 Myr. Using these ages, the models imply masses of 0.005–0.015 $M_\odot$ for the four ≥M9 members. In the IMFs, I divide these objects evenly between the two mass bins on either side of 0.01 $M_\odot$. The resulting IMFs for the $1.5^\circ \times 0.35^\circ$ and $0.22^\circ \times 0.28^\circ$ fields are presented in Figure 15. For comparison, I include the similarly derived IMFs for Taurus (Luhman 2004d) and IC 348 (Luhman et al. 2003b). For these IMF samples from Chamaeleon I, Taurus, and IC 348, I also show the distributions of spectral types and dereddened absolute *H*-band magnitudes in Figures 16 and 17, respectively.

4.3. *Turnover Mass*

Notable features to examine in the IMF of a young cluster are the mass at which it reaches a maximum, the relative numbers of

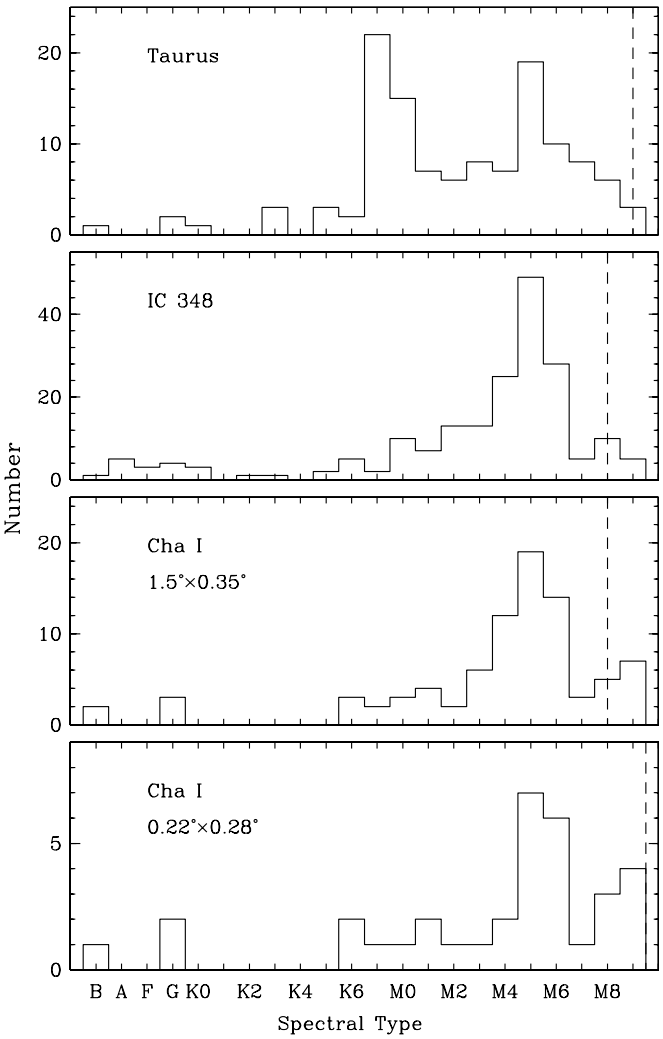


FIG. 16.—Distributions of spectral types for the IMFs in Fig. 15. The completeness limits of these samples are indicated (*dashed lines*).

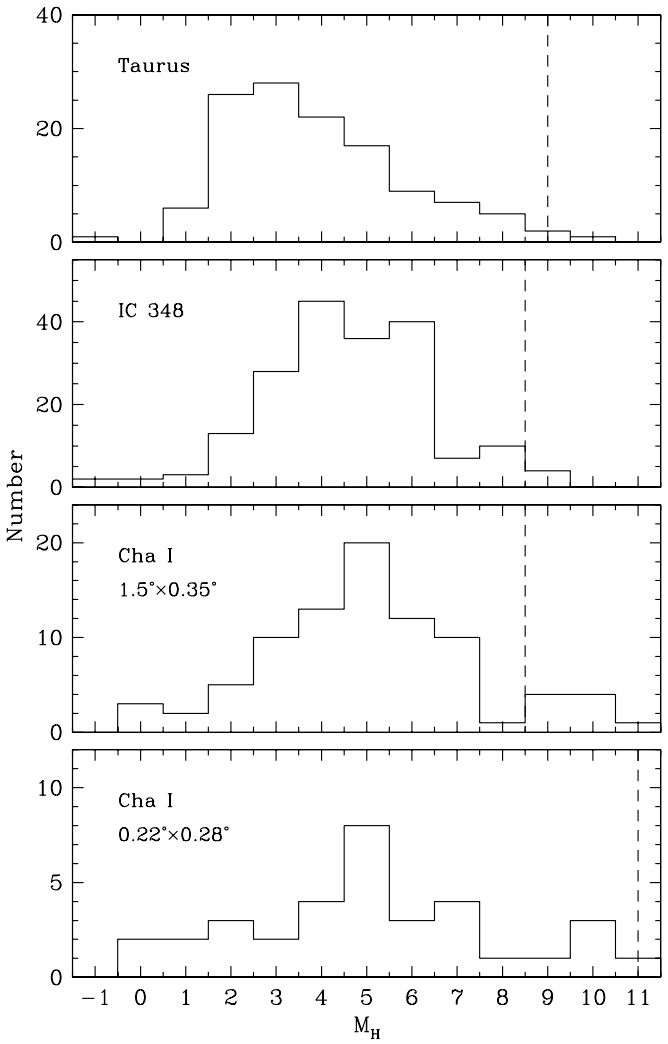


FIG. 17.—Distributions of *H*-band magnitudes for the IMFs in Fig. 15, corrected for extinction and distance. The completeness limits of these samples are indicated (*dashed lines*).

objects in different mass ranges, and the minimum mass. Because it contains more objects, the IMF in the $1.5^\circ \times 0.35^\circ$ field provides a better measurement of the first two properties, while the deeper IMF in the $0.22^\circ \times 0.28^\circ$ area better constrains the minimum mass of the IMF.

The mass at which the IMF reaches a maximum has been shown to vary significantly between the low-density stellar population in Taurus ($M \sim 0.8\ M_\odot$; Luhman 2000, 2004d; Briceño et al. 2002) and the denser clusters of IC 348 in Perseus and the Orion Nebula Cluster ($M \sim 0.1$–$0.2\ M_\odot$ Hillenbrand 1997; Hillenbrand & Carpenter 2000; Muench et al. 2002, 2003; Luhman et al. 2003b). The peak mass of the $1.5^\circ \times 0.35^\circ$ IMF in Chamaeleon I is 0.1–0.15 $M_\odot$, which is similar to the value in IC 348, as shown in Figure 15. The agreement between Chamaeleon I and IC 348 is also apparent in the distributions of spectral types and M_H in Figures 16 and 17, respectively. Meanwhile, Taurus is distinct from both clusters in all of these diagrams. Thus, the characteristic mass of the IMF exhibits no noticeable variation among Orion, Chamaeleon, and Perseus. With a peak mass near 0.8 $M_\odot$, Taurus remains unique among well-studied nearby star-forming regions. As discussed by Briceño et al. (2002) and Luhman et al. (2003b), the distinctive nature of the IMF in Taurus may be a reflection of an unusually high average Jeans mass.

4.4. *Minimum Mass*

To date, measurements of IMFs in nearby star-forming regions have reached mass limits of $\sim$0.005–0.02 $M_\odot$ through luminosity-function modeling (Luhman et al. 2000; Hillenbrand & Carpenter 2000; Muench et al. 2002, 2003; Preibisch et al. 2003; Lucas et al. 2005) and spectroscopy (Hillenbrand 1997; Comerón et al. 2000; Béjar et al. 2001; Luhman et al. 2003b; Briceño et al. 2002; Barrado y Navascués et al. 2004; Luhman 2004d; Slesnick et al. 2004; Levine et al. 2006; Lucas et al. 2006). Individual brown dwarfs that are not part of IMF measurements have also been found near masses of $\sim$0.01 $M_\odot$ (Kirkpatrick et al. 2006; Allers et al. 2006, 2007). The best constraints on the minimum mass in Chamaeleon I are provided by my survey of a $0.22^\circ \times 0.28^\circ$ field in the southern subcluster. The IMF for this field extends down to the completeness limit of $\sim$0.01 $M_\odot$ and perhaps even to 0.005 $M_\odot$. Thus, the minimum mass of the IMF in Chamaeleon I is $<$0.01 $M_\odot$, which is comparable to constraints provided by IMF measurements in a few other young clusters. In comparison, a minimum mass of 0.001–0.01 $M_\odot$ has been predicted by calculations of opacity-limited fragmentation (Low & Lynden-Bell 1976; Rees 1976; Silk 1977; Boss 1988; Bate 2005; Whitworth & Stamatellos 2006). To better constrain these

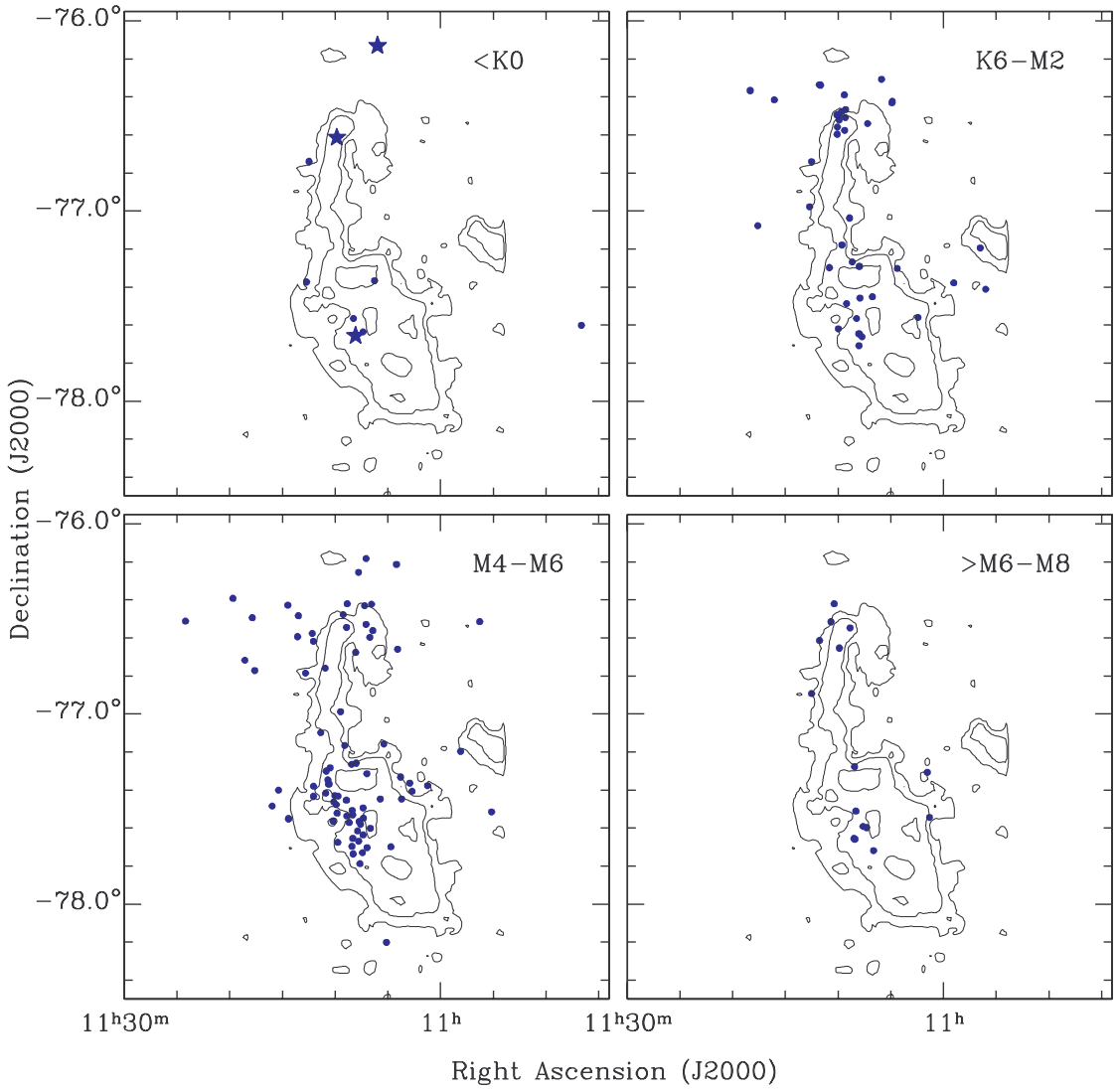


FIG. 18.—Spatial distributions of members of Chamaeleon I for different ranges of spectral types. The three B stars are indicated (*stars*). The contours represent the extinction map of Cambrésy et al. (1997) at intervals of $A_J = 0.5$, 1, and 2.

predictions with Chamaeleon I, a survey with a deeper completeness limit is required.

4.5. *Brown Dwarf Fraction*

As done in Briceño et al. (2002) and Luhman et al. (2003b), I quantify the relative numbers of brown dwarfs and stars in Chamaeleon I with the following ratio:

$$R_1 = \frac{N(0.02 \leq M/M_\odot \leq 0.08)}{N(0.08 < M/M_\odot \leq 10)}.$$

For the $1.5^\circ \times 0.35^\circ$ IMF, this ratio is $R_1 = 16/62 = 0.26^{+0.06}_{-0.05}$. This brown dwarf fraction for Chamaeleon I is higher than measurements in IC 348 and Taurus by a factor of 1.5–2 (Briceño et al. 2002; Luhman et al. 2003a, 2003b; Luhman 2004d) and is similar to values reported for Orion (Luhman et al. 2000; Hillenbrand & Carpenter 2000; Muench et al. 2002; Slesnick et al. 2004). The variations among these ratios are significant if only the formal statistical errors are considered. However, it is likely that additional systematic errors are present in these measurements. In particular, because the peak of the IMF is close to the hydrogen-burning limit (see Figs. 15 and 16), small systematic offsets in mass estimates can result in large differences in the relative numbers of stars and brown dwarfs. These offsets can arise from differences in adopted evolutionary models, temperature scales, and spectral classification systems (Luhman 2006), or from basic differences in the methods of estimating masses (e.g., positions on H-R diagrams vs. luminosity functions). These sources of systematic errors are not present among the measurements that I have performed in IC 348, Taurus, and Chamaeleon I. However, because the low-mass stars in IC 348 and Chamaeleon I are segregated and low-mass stars dominate these stellar populations by number, the brown dwarf fraction is also sensitive to the size of the field in which it is measured. The fields considered in IC 348, Taurus, and Chamaeleon I are probably large enough to accurately represent the entire stellar population in each cluster, but it is possible that the brown dwarf fractions would change noticeably if they were measured from even larger fields. Even in the absence of systematic errors, the modest differences in the brown dwarf fractions of these regions can be explained by slight variations in the peak mass of the IMF and probably do not require a deeper explanation that is specific to brown dwarf formation.

5. SPATIAL DISTRIBUTION

5.1. *Brown Dwarfs within 3°*

If I account for the completeness limits described in § 2.4, I can use the current census of Chamaeleon I to characterize the spatial distribution of stars and brown dwarfs in this cluster. I first investigate whether a widely distributed population of brown dwarfs is present in Chamaeleon I. The IK2 survey was specifically designed for this question (§ 2.1.2). To be sensitive to members moving at high velocities ($v \gtrsim 2$ km s^{-1}), such as brown dwarfs ejected from multiple systems (Reipurth & Clarke 2001), I selected a search radius of 3° from the center of Chamaeleon I, which corresponds to the angular distance traveled by an object moving at 8 km s^{-1} in the plane of the sky at the distance of Chamaeleon I for a duration of 1 Myr. I also considered only sources with $i - K_s > 2.5$ ($\gtrsim$M4.5), which is blue enough to encompass the peak of the spectral-type distribution of the cluster (Fig. 16) while red enough to minimize contamination by field stars (Fig. 3). As demonstrated in § 2.4, the IK2 survey is complete for substellar cluster members above masses of 0.03 $M_\odot$ ($\lesssim$M8) that are within areas covered by the Second DENIS Release (Fig. 1).

As shown in the map of known members of Chamaeleon I in Figure 1*b*, a population of widely distributed brown dwarfs is not present out to a radius of 3° (8.5 pc) surrounding the cluster. To quantify this result, I compare the relative numbers of low-mass stars and brown dwarfs between the inner and outer regions of the cluster. The ratio N(>M6–M8)/N(M4.5–M6) is $1/12 = 0.08^{+0.15}_{-0.02}$ for $1.25° < r \leq 3°$, which is actually lower than the value of $15/70 = 0.21^{+0.06}_{-0.05}$ for $r \leq 1.25°$.

Several studies have suggested that brown dwarfs form by the ejection of protostellar sources from multiple systems (Reipurth & Clarke 2001; Boss 2001; Bate et al. 2002; Delgado-Donate et al. 2003; Umbreit et al. 2005; Goodwin & Whitworth 2007). Some of these models predict that brown dwarfs are born with higher velocity dispersions than stars and consequently have wide spatial distributions in star-forming regions (Reipurth & Clarke 2001; Kroupa & Bouvier 2003). However, I have shown that brown dwarfs are not more widely distributed than their stellar counterparts in Chamaeleon I. Luhman (2006) and Slesnick et al. (2006) found the same result for Taurus, which also lacks an extended population of brown dwarfs. Thus, embryo ejection models that predict high velocities for brown dwarfs are not viable as the dominant mode of brown dwarf formation.

5.2. *Stars and Brown Dwarfs within 1°*

I next examine the spatial distributions of members of Chamaeleon I within a radius of ~1° from the cluster center. Because I wish to compare the distributions for different ranges of spectral types, I begin by summarizing the completeness within this area (§ 2.4). The current census of the central $1.5° \times 0.35°$ field should be nearly 100% complete for $M/M_\odot \geq 0.03$ ($\lesssim$M8) and $A_J \leq 1.2$. Outside of this field, most members at M4.5–M8 should be identified. Members later than M8 are excluded from this analysis of spatial distributions because only the central regions of the two subclusters in Chamaeleon I have been thoroughly searched at such late types. The completeness at types earlier than mid-M is not well-determined outside of the $1.5° \times 0.35°$ field, but it is likely that wide-field X-ray and Hα surveys have found most of the earlier members, particularly given the low levels of extinction outside of the $1.5° \times 0.35°$ field. Thus, spatial distributions measured from members earlier than M8 in the current census should be accurate representations of the cluster.

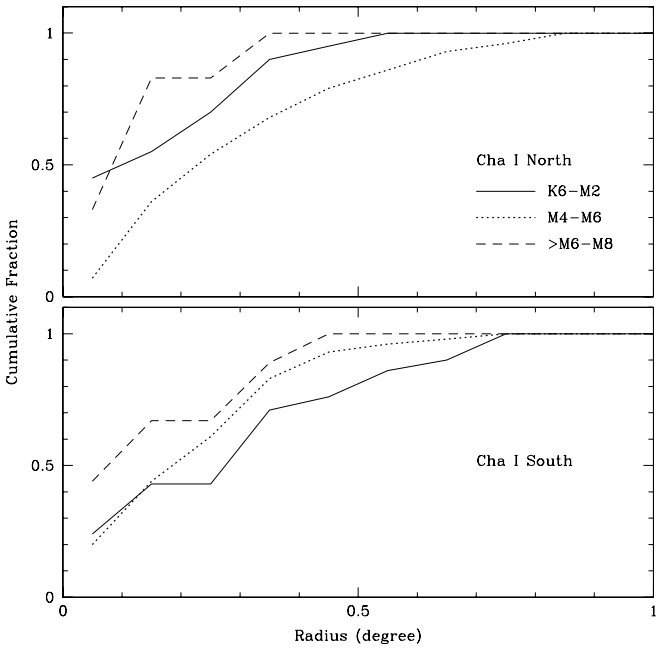


FIG. 19.—Cumulative distributions of projected angular radii from the centers of the northern (*top*, $\delta > -77°$) and southern (*bottom*, $\delta < -77°$) subclusters in Chamaeleon I for members with spectral types of K6–M2 (*solid lines*), M4–M6 (*dotted lines*), and >M6–M8 (*dashed lines*). The centers are defined as the positions of the maximum surface densities, corresponding to $\alpha = 11^h09^m40^s$, $\delta = -76°33'00''$ and $\alpha = 11^h08^m00^s$, $\delta = -77°38'00''$ (J2000) for the northern and southern subclusters, respectively. An outer radius of 1° was adopted for each subcluster.

To characterize the spatial distribution of the stellar population of Chamaeleon I as a function of mass, I first plot the positions of members with spectral types of <K0, K6–M2, M4–M6, and >M6–M8 on separate maps in Figure 18. The cluster contains too few stars at <K0 to examine their spatial distribution in detail. I only note that two of the three most massive members, the B stars T32 and T41, are located near the centers of the two subclusters, which is often the case in young clusters (Hillenbrand & Hartmann 1998 and references therein). The third B star, HD 96675, is north of the Chamaeleon I cloud (see Fig. 18). In § 3.3, I suggested that the it may have formed from a small cloudlet that has recently dissipated.

Based on visual inspection of Figure 18, the members at K6–M2, M4–M6, and >M6–M8 exhibit similar spatial distributions in the southern subcluster. However, in the northern subcluster, the M4–M6 members appear to have a significantly wider distribution than the objects at K6–M2 and >M6–M8. To quantitatively assess this possible mass segregation, I have computed the cumulative distributions of radii from the centers of the northern and southern subclusters for K6–M2, M4–M6, and >M6–M8, which are shown in Figure 19. Again, the northern M4–M6 members are less centrally concentrated than the other populations. According to two-sided Kolmogorov-Smirnov tests among the northern radial distributions, the probability that the M4–M6 sample is drawn from the same parent distribution as K6–M2 and >M6–M8 is 1%–2%, while the latter two samples are consistent with each other. Meanwhile, no significant differences are present among the three radial distributions in the southern subcluster.

Mass segregation of the kind found in the northern subcluster has been reported in other young clusters such as IC 348 (Muench et al. 2003) and the Orion Nebula Cluster (Hillenbrand & Carpenter 2000). In each of those clusters, the peak mass of the IMF varies

from $\sim$0.5 $M_\odot$ in the core to $\sim$0.1 $M_\odot$ at large radii. Dynamical cluster evolution is not a plausible source of the mass segregation of low-mass stars in IC 348 and Orion, and it is even less likely at the lower stellar densities found in Chamaeleon I. Instead, it would seem that the mass segregation in these clusters must be primordial. However, it is unclear why the southern subcluster shows no segregation. Measurements of velocities for the members of Chamaeleon I and an analysis of their dependence on mass and position would likely prove to be valuable in further exploring this issue.

5.3. *Constraints on Star Formation History*

The spatial distribution of members of Chamaeleon I can also be used to constrain the star formation history. To search for a widely distributed population of members, Covino et al. (1997) measured Li absorption strengths and radial velocities for X-ray sources from the *ROSAT* all-sky survey within 170 deg^2 surrounding the Chamaeleon complex of clouds. They identified 37 pre–main-sequence stars, which exhibited spectral types of late G to early M. Complimenting that study, my wide-field survey (IK2, § 2.1.2) considers a smaller area but reaches lower masses and most importantly encompasses the peak of the IMF. These two surveys indicate that few young stars reside at large distances from the Chamaeleon I cloud.

Feigelson (1996) suggested that star formation has occurred at a constant rate for 20 Myr in Chamaeleon I and that the observed deficit of older stars ($\tau \gtrsim 2$ Myr) in this cluster and other star-forming regions is caused by the dispersal of the older stars. However, in contrast to the expectations of that scenario, the wide-field surveys with *ROSAT* (Alcalá et al. 1995, 1997; Covino et al. 1997) and in this work have shown that the Chamaeleon I clouds are not surrounded by a large population of young stars. Similar results have been found for other star-forming regions (Briceño et al. 1997). In addition, the distributions of isochronal ages in Figure 14 are inconsistent with a constant star formation rate for 10–20 Myr.

6. CONCLUSIONS

I have presented an extensive search for new members of the Chamaeleon I star-forming region. Because the completeness limits of my survey are well-determined, I have been able to perform robust measurements of the distributions of members of Chamaeleon I as a function of mass, position, and age. The primary results of this study are summarized as follows:

1. I have discovered 50 new members of Chamaeleon I, which increases the census of known members to 226 objects. The new members include 14 objects that are later than M6 ($M \lesssim 0.08\ M_\odot$) and the two faintest known members of the cluster, which may have masses of only 0.005–0.01 $M_\odot$. The current census now contains 28 members that are likely to be substellar.

2. The distribution of isochronal ages for members of Chamaeleon I between 0.1 and 1 $M_\odot$ suggests that star formation has occurred for the past 3–4 and 5–6 Myr in the southern and northern subclusters, respectively, at rates that have declined with time.

3. The IMF in Chamaeleon I reaches a maximum at a mass of 0.1–0.15 $M_\odot$, which is similar to the turnover mass observed in IC 348 and the Orion Nebula Cluster (Hillenbrand 1997; Hillenbrand & Carpenter 2000; Muench et al. 2002, 2003; Luhman et al. 2003b). The substellar IMF is roughly flat in logarithmic units and shows no indication of reaching a minimum down to a completeness limit of 0.01 $M_\odot$.

4. Chamaeleon I does not contain a widely distributed population of brown dwarfs, which is contrary to the predictions of some embryo-ejection models. Instead, the substellar members share the same spatial distribution as the stars. However, low-mass stars in the northern subcluster do appear to have a wider distribution than members at other masses, which resembles the mass segregation that has been previously observed in Orion and IC 348 (Hillenbrand & Carpenter 2000; Muench et al. 2003).

I thank the staff at Las Campanas Observatory for their assistance with these observations and Eric Feigelson and Eric Mamajek for helpful comments on the manuscript. This work was supported by grant NAG5-11627 from the NASA Long-Term Space Astrophysics program and grant GO-10138 from the Space Telescope Science Institute. This publication makes use of data products from 2MASS, which is a joint project of the University of Massachusetts and the Infrared Processing and Analysis Center/California Institute of Technology, funded by NASA and the NSF. The DENIS project has been partly funded by the SCIENCE and the HCM plans of the European Commission under grants CT920791 and CT940627. It is supported by INSU, MEN, and CNRS in France, by the State of Baden-Württemberg in Germany, by DGICYT in Spain, by CNR in Italy, by FFwFBWF in Austria, by FAPESP in Brazil, by OTKA grants F-4239 and F-013990 in Hungary, and by the ESO C&EE grant A-04-046. J. C. Renault from IAP was the Project manager. Observations were carried out thanks to the contribution of numerous students and young scientists from all involved institutes, under the supervision of P. Fouqué.

APPENDIX A

COMMENTS ON INDIVIDUAL SOURCES

The strengths of the gravity-sensitive lines in the spectra of 2MASS 10555824−7418347 and 10435748−7633023 appear to be intermediate between those of field dwarfs and known Chamaeleon I members, indicating that these objects may be young members of the field. Similar objects have been identified toward the Taurus cloud complex (Luhman 2006; Slesnick et al. 2006) and in the solar neighborhood (Cruz et al. 2007).

The spectra of ISO 217 from Luhman (2004a) and from 2004 January are similar, but the spectrum from 2005 January for this object exhibits stronger emission lines, brighter blue continuum, and weaker TiO than those two earlier spectra. All of these characteristics are consistent with an increase in the accretion rate. Similar variability is present in the data for Cha Hα 1 and T48, as shown in Figure 20. The variability for T48 occurred over a period of only 3 days.

ESO Hα 281 was resolved as a 1.7″ pair by Reipurth & Zinnecker (1993). The brighter component was designated as ESO Hα 281A by Brandner & Zinnecker (1997) and is 2MASS 11070350−7631443. The spectral classifications from Brandner & Zinnecker (1997) and in this work indicate that this star is a background giant. The fainter component, ESO Hα 281B from Brandner & Zinnecker (1997)

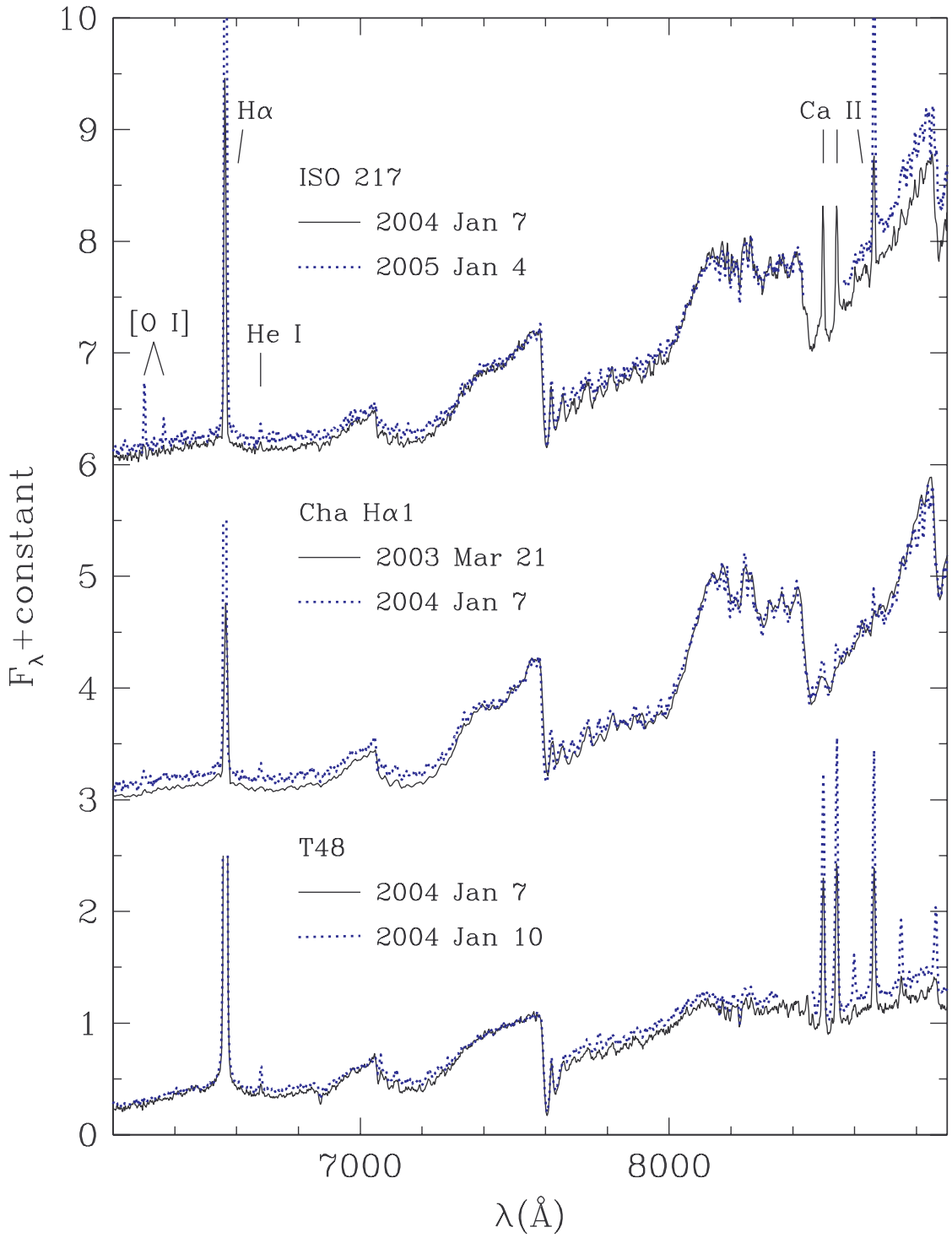


FIG. 20.—Chamaeleon I members that exhibit variability in their spectra. For each object, an increase in Hα and other emission lines is accompanied by brighter continuum emission and weaker absorption bands at blue wavelengths, which are indicative of veiling by blue excess emission. The data are normalized at 7500 Å.

is not resolved from the brighter star by 2MASS. It was spectroscopically confirmed as a member of Chamaeleon I by Brandner & Zinnecker (1997), but it was overlooked in the compilation of members in Luhman (2004a).

The spectrum of 2MASS 11253653−7700348 has M-type spectral features but does not match any standard dwarfs, giants, or pre–main-sequence objects. Thus, the luminosity class of this object is uncertain. It is unlikely to be a young star based on the absence of Li absorption in its spectrum.

The strengths of the Na I and K I lines in the spectrum of 2MASS 11052472−7626209 are suggestive of youth. However, because the variation of these lines between dwarfs and pre–main-sequence stars is subtle for the spectral type of this star (M2.75), it remains possible that it is a field dwarf. Similarly, the triangular *H*-band continuum of Cha J11083040−7731387 is indicative of youth (Lucas et al. 2001), but this object appears to have strong K I absorption at 1.25 μm, which suggests higher, dwarflike gravity. Because no

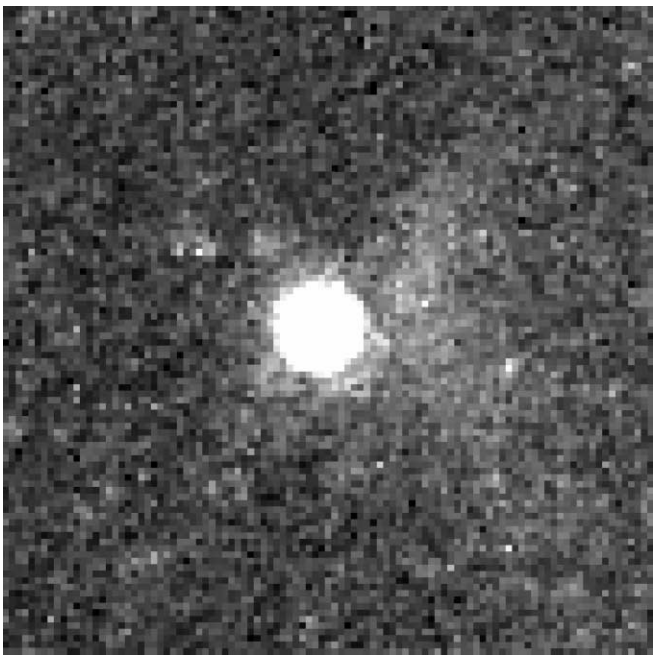


FIG. 21.—ACS F775W image of Cha J11081938−7731522. The presence of extended emission and its butterfly morphology indicate that this star is seen in scattered light (e.g., edge-on disk), which is consistent with its subluminous nature (Figs. 5 and 11). The size of the image is $5'' \times 5''$.

spectral type of field M and L dwarfs matches the spectrum of Cha J11083040−7731387 and the apparent strength of K I may be due to a low signal-to-noise ratio, I assume that it is a member of Chamaeleon I for the purposes of this work.

Saffe et al. (2003) presented an optical spectrum for a putative new member of Chamaeleon I. They attributed their spectrum to 2MASS 11095300−7730588 and named the object SGR1. Their spectrum exhibited strong Hα emission, and they reported a spectral type of M7 from those data. However, my spectrum of this star shows no Hα emission or late-type molecular bands and instead is indicative of a reddened background field star. If placed on the color-magnitude diagram in Figure 4 ($R - I = 1.4$, $I = 18.7$), this star falls well below the sequence of known members, which further indicates that it is a field star rather than a member. Finally, SGR 1 should have a circumstellar disk if it has the strong Hα emission found by Saffe et al. (2003). However, SGR 1 does not exhibit the excess emission expected from a disk in mid-IR images from Luhman et al. (2005b). The spectrum published by Saffe et al. (2003) (from multiobject spectroscopy) was probably incorrectly associated with 2MASS 11095300−7730588 and in fact may apply to a previously known member.

Six known members of Chamaeleon I appear below the main sequence in the H-R diagram in Figure 13, consisting of CHSM 15991, T14A, ISO 225, ESO Hα 569 and 574, and Cha J11081938−7731522. Low luminosity estimates were also derived by Luhman (2004a) for the first three stars and by Comerón et al. (2004) for ESO Hα 569 and 574. Luhman (2004a) suggested that CHSM 15991, T14A, and ISO 225 are unusually faint because they are seen only in scattered light (e.g., edge-on disks), and Comerón et al. (2004) offered the same explanation for ESO Hα 574. Comerón et al. (2004) concluded that ESO Hα 569 is more likely to have an intrinsically low luminosity rather than an edge-on disk because excess emission from a disk was not detected in mid-IR observations with ISO (Persi et al. 2000). However, ESO Hα 569 does exhibit strong excess emission in the *Spitzer* data from Luhman et al. (2005b). The absence of a detection of this star in the X-ray images from Feigelson & Lawson (2004) can be used to constrain the amount of extinction toward the star. If ESO Hα 569 has an X-ray luminosity in the range of values observed for classical T Tauri stars at masses of 0.4 $M_{\odot}$ (Telleschi et al. 2007), then the detection limit described by Feigelson & Lawson (2004) indicates an extinction of $A_K \gtrsim 60$ toward this star. Thus, the X-ray data from Feigelson & Lawson (2004) support the presence of an edge-on disk around ESO Hα 569. The sixth star below the main sequence in Figure 13, Cha J11081938−7731522, is newly identified as a cluster member in this work. It also appears subluminous in Figures 4, 5, and 11. Although it falls below the sequences of known members in those diagrams, Cha J11081938−7731522 was not rejected as a field star because it was red enough in Figure 4 to be selected as a candidate (substellar) member. The presence of extended emission around this star in the ACS image in Figure 21 supports the idea that it is seen in scattered light. In particular, the shape of the emission resembles the butterfly morphology that characterizes edge-on disks.

Kraus & Hillenbrand (2007) presented a tabulation of 14 candidate wide companions to known members of Chamaeleon I. My photometry and spectroscopy provide new constraints on the cluster membership of some of these candidates. Through spectroscopy, I have classified the candidate brown dwarf companion to ISO 250, 2MASS 11103749−7722083, as a field star. Note that this candidate is different from the candidate companion to ISO 250 that was found by López Martí et al. (2004). I also have spectroscopically classified the candidate near KG 102 as a field star. The candidate companions to C7-1 and T14A are below the cluster sequence in Figure 4 ($I = 18.1$ and 18.4, $R - I = 1.8$ and 0.8, respectively), indicating that they are probably not members of the cluster. The candidate companions to T3 and T26 are spectroscopically confirmed as members in this work. The candidate companion to T39A+B, 2MASS 11091297−7729115, is a candidate member according to my color-magnitude diagrams. It is the one remaining bright candidate appearing in Figure 10. Although it was included in the list of candidate companions from Kraus & Hillenbrand (2007), the candidate near T33 was already confirmed as a cluster member by previous studies (e.g., Luhman 2004a).

APPENDIX B

COMPARISON TO PREVIOUS SURVEYS

B1. FEIGELSON & LAWSON (2004) AND STELZER ET AL. (2004)

Using the *Chandra X-ray Observatory*, Feigelson & Lawson (2004) obtained an image of a $16' \times 16'$ field in the northern subcluster of Chamaeleon I, which is indicated in Figure 1*a*. They detected 27 previously known members and identified no new candidate members. Feigelson & Lawson (2004) concluded that the census of known members in their survey field is complete to masses of $\sim 0.1\ M_{\odot}$. The membership classifications based on the X-ray data from Feigelson & Lawson (2004) agreed well with the classifications by Luhman (2004a) using other diagnostics. ISO 165 was the only star that was classified differently between the two studies. Luhman (2004a) classified ISO 165 as a member of Chamaeleon I because of its strong Hα emission ($W_{\lambda} = 49 \pm 3$) and weak Na I and K I lines that are indicative of low surface gravity. In addition, it cannot be a foreground dwarf because it significantly reddened, while it cannot be a background dwarf because such an object would appear below the main sequence when placed on the H-R diagram at the distance of Chamaeleon I, which is not the case. In comparison, Feigelson & Lawson (2004) suggested that ISO 165 might be a nonmember because it was not detected in their X-ray data. However, the spectral type of M5.5 for this object corresponds to a mass of $0.1-0.15\ M_{\odot}$, which is near their completeness limit, so it is not surprising that it was not detected. In the mid-IR images from Luhman et al. (2005b), ISO 165 exhibits mid-IR excess emission that indicates the presence of a disk, which provides further evidence of the youth and membership of this object in Chamaeleon I. In addition to ISO 165, seven other known members of Chamaeleon I were not detected in the X-ray data from Feigelson & Lawson (2004). Six of these sources have spectral types later than M7 ($M \lesssim 0.06\ M_{\odot}$), and thus detections were not expected since they fall below the mass completeness limit of the X-ray data. The seventh member, ESO Hα 569 (Comerón et al. 2004), has a relatively high mass of $0.4\ M_{\odot}$ based on its spectral type of M2.5, and yet it was not detected by Feigelson & Lawson (2004) which suggests the presence of extremely high extinction toward this star ($A_K \gtrsim 60$; Appendix A).

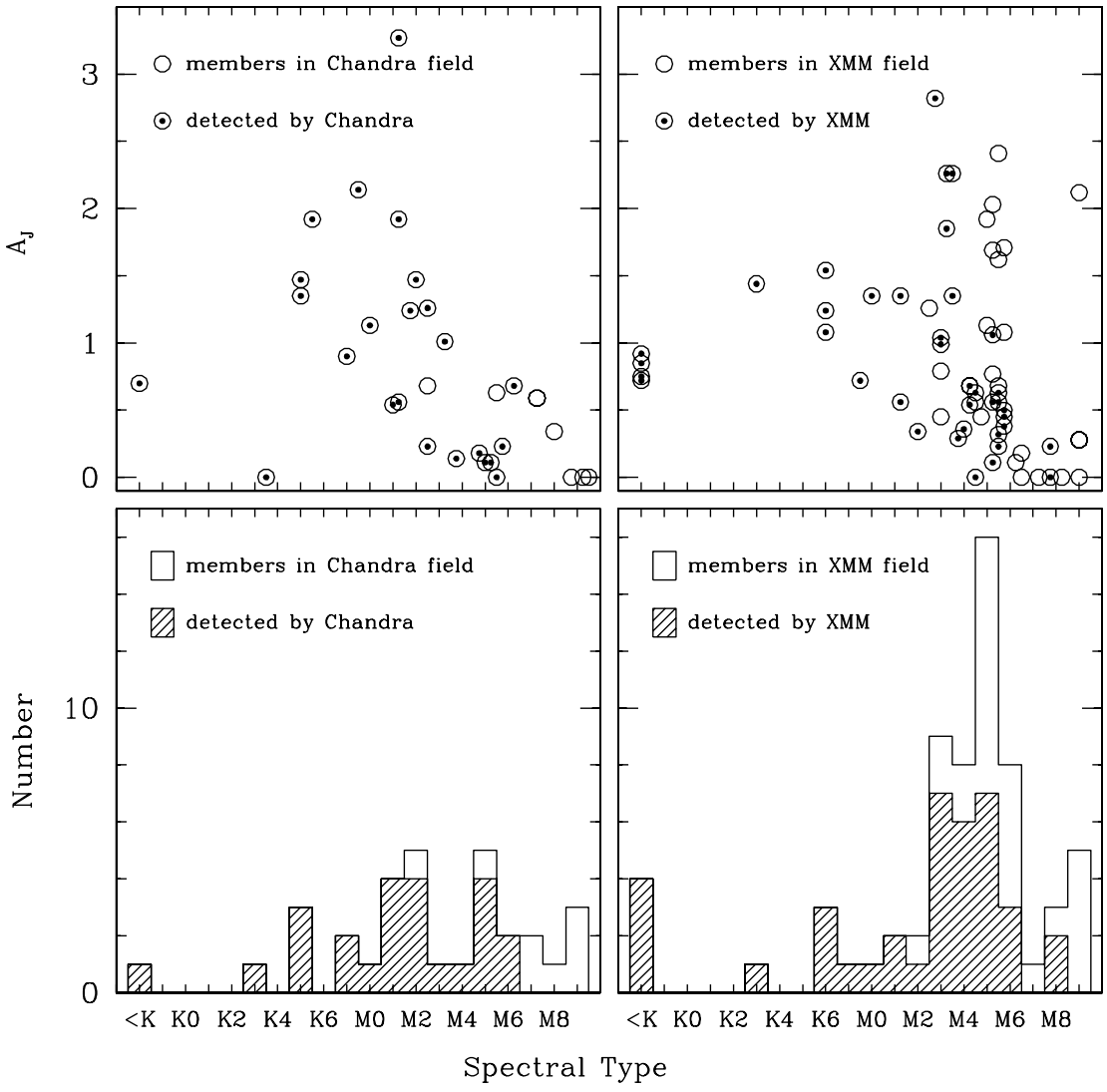


FIG. 22.— Extinctions (*top*) and spectral types (*bottom*) for the known members of Chamaeleon I (*circles and histograms*) within the *Chandra* (*left*) and *XMM* (*right*) fields shown in Fig. 1*a*. The members detected by these X-ray telescopes are indicated (*circled points and hatched histograms*).

Using *XMM-Newton*, Stelzer et al. (2004) obtained an X-ray image of a $27' \times 27'$ field in the southern subcluster of Chamaeleon I, which is indicated in Figure 1*a*. Their image encompassed 71 of the known members in the current census of Chamaeleon I (§ 2.3), 38 of which were detected. One of the X-ray sources from Stelzer et al. (2004), HD 97240 (KG 2001-78), was treated as a possible member of Chamaeleon I in that study. However, it is probably a foreground star rather than a cluster member based on its proper motion and parallax (Whittet et al. 1987; Perryman et al. 1997).

To investigate the completeness of the X-ray observations by Feigelson & Lawson (2004) and Stelzer et al. (2004) I show in Figure 22 the distributions of spectral types for all known members of Chamaeleon I within each survey field and for the members detected in X-rays. Five and three of the known members in the *XMM-Newton* and *Chandra* fields, respectively, are not included in the histograms because accurate spectral types are not available for them. According to Figure 22, the *XMM-Newton* data are complete for spectral types earlier than M2 ($M \gtrsim 0.5\ M_{\odot}$), and the level of completeness steadily decreases with later types. In comparison, the completeness of the *Chandra* image from Feigelson & Lawson (2004) changes more abruptly and remains close to 100% down to ~M6. To examine the origin of the differences in completeness limits between these two X-ray studies, I have included in Figure 22 my estimates of A_J as function of spectral type. At M5–M6, the members that were not detected by *XMM-Newton* have systematically higher extinctions than the detected members, indicating that extinction prevented their detection. Most of the nondetections at earlier types were too close to brighter stars to be resolved by *XMM-Newton*, including T39B, T30, and 2MASS 11072022−7738111. Compared to the *XMM-Newton* field, the extinction from the cloud decreases more rapidly from the center to the edge of the *Chandra* field, as shown in Figure 1. Because the low-mass stars are distributed more widely than the high-mass stars in the northern subcluster of Chamaeleon I (§ 5),[3] they are subjected to lower extinction in the *Chandra* field than in the *XMM-Newton* field. As a result, *Chandra* was able to detect a higher fraction of M5–M6 stars than *XMM-Newton*.

Feigelson & Lawson (2004) measured an IMF from the sample of members detected in their *Chandra* data. Their IMF exhibited a significant deficiency of low-mass stars ($0.1-0.3\ M_{\odot}$) relative to the Orion Nebula Cluster (Hillenbrand 1997; Hillenbrand & Carpenter 2000; Muench et al. 2002). The same deficiency is present when the *Chandra* field is compared to the *XMM-Newton* field in the southern subcluster and the larger $1.5^{\circ} \times 0.35^{\circ}$ area in Chamaeleon I, as shown in Figures 16 and 22. The membership lists from Feigelson & Lawson (2004) and this work agree almost perfectly down to M6, or $0.1\ M_{\odot}$, so this effect is not a result of incompleteness in the *Chandra* data. Indeed, my census is complete to much lower masses for most of the *Chandra* field, and it still exhibits the deficit of low-mass stars (Fig. 22). Instead of incompleteness, the anomalous IMF in the *Chandra* field is a reflection of the segregation of low-mass stars to larger radii surrounding the northern subcluster that was described in § 5.

B2. LÓPEZ MARTÍ ET AL. (2004)

López Martí et al. (2004) obtained images in R, I, Hα, and two narrowband optical filters toward 1.2 deg^2 in Chamaeleon I. With these data, they identified 69 candidate members of the cluster. They selected three additional stars as candidates based on X-ray emission and IR excess emission. Among these 72 candidates, 50 objects were spectroscopically classified as members by Luhman (2004a) and Comerón et al. (2004), and 10 objects have been classified as members in this work. Four candidates are field stars based on my spectroscopy (Table 4). The remaining eight candidates lack accurate spectral classifications, consisting of sources 424, 427, 428, 441, 607, 618, 619,

[3] For Chamaeleon I members within the *Chandra* image, the average distances from the center of the image are 3.5′ and 7′ for spectral types of <M3 and M3–M6, respectively.

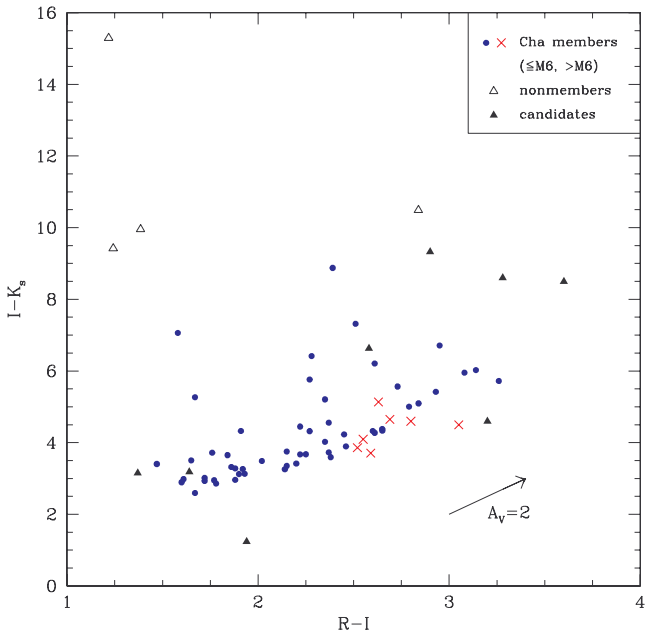


FIG. 23.—Color-color diagram for the candidate members of Chamaeleon I identified by López Martí et al. (2004). Most of these stars have been spectroscopically classified as members (*circles and crosses*) or nonmembers (*triangles*) in this work and in previous studies. Only one of the remaining unclassified candidates exhibits colors that are indicative of a late-type (>M6) member.

and 749 from López Martí et al. (2004). The first five objects were classified as late M or early L by López Martí et al. (2004) through their optical colors, while the latter three candidates exhibited bluer colors indicative of <M4. These candidates were originally identified by López Martí et al. (2004) through a diagram of I versus $R - I$; their candidacy can be further refined by plotting them in a diagram of $I - K_s$ versus $R - I$ (Luhman 2001). In Figure 23, I show this diagram for the 72 candidates from López Martí et al. (2004), which are divided into members at ≤M6 and >M6, nonmembers, and the eight candidates that lack spectral classifications. In the latter group, the five objects with the reddest colors are those classified as late M or L by López Martí et al. (2004). Only source 424 exhibits colors that are consistent with those of the confirmed late-type members. The other four candidates are too red in $I - K_s$ for their $R - I$, which suggests that they are highly reddened early-type objects rather than late-type sources. This conclusion is supported by the near-IR spectra of sources 428 and 607 from Gómez & Mardones (2003) which lack the strong steam absorption that is expected for late M and L types.

López Martí et al. (2004) estimated spectral types for their 72 candidates from optical colors. The classifications of 29 candidates were later than M6. In comparison, 15 and 7 of these 29 objects have been spectroscopically classified as members with types of ≤M6 and >M6, respectively. Three late-type candidates are field stars according to my spectroscopy, and three candidates are likely to have earlier types based on their positions in Figure 23 and the absence of steam absorption in the spectra from Gómez & Mardones (2003), while source 424 remains a viable late-type candidate. Thus, no more than 8 of the 29 objects that were classified as later than M6 by López Martí et al. (2004) actually have spectral types in this range. It is likely that the types from López Martí et al. (2004) were systematically too late because of extinction. When estimating spectral types from the colors of their candidates, López Martí et al. (2004) did not correct for extinction, which was unknown without spectroscopic data. Because some of their candidates were field stars and their spectral types exhibited systematic errors, the validity of the IMF derived from that sample of candidates by López Martí et al. (2004) is questionable.

B3. COMERÓN ET AL. (2004)

Comerón et al. (2004) performed an Hα survey across all of Chamaeleon I and obtained spectroscopy of candidate members appearing in those images. They discovered 18 new members of the cluster, seven and eight of which were independently found by Luhman (2004a) and this study. The spectral types from Comerón et al. (1999, 2000, 2004) and Neuhäuser & Comerón (1999) are systematically later than those from Luhman (2004a) and this work by an average of 0.5 subclasses.

REFERENCES

Adams, F. C., & Fatuzzo, M. 1996, ApJ, 464, 256
Alcalá, J. M., Krautter, J., Covino, E., Neuhäuser, R., Schmitt, J. H. M. M., & Wichmann, R. 1997, A&A, 319, 184
Alcalá, J. M., Krautter, J., Schmitt, J. H. M. M., Covino, E., Wichmann, R., & Mundt, R. 1995, A&AS, 114, 109
Allers, K. N., Kessler-Silacci, J. E., Cieza, L. A., & Jaffe, D. T. 2006, ApJ, 644, 364
Allers, K. N., et al. 2007, ApJ, 657, 511
Appenzeller, I. 1979, A&A, 71, 305
Appenzeller, I., Jankovics, I., & Krautter, J. 1983, A&AS, 53, 291
Baraffe, I., Chabrier, G., Allard, F., & Hauschildt, P. H. 1998, A&A, 337, 403
Barrado y Navascués, D., Stauffer, J. R., Bouvier, J., Jayawardhana, R., & Cuillandre, J.-C. 2004, ApJ, 610, 1064
Bate, M. R. 2005, MNRAS, 363, 363
Bate, M. R., Bonnell, I. A., & Bromm, V. 2002, MNRAS, 332, L65
Béjar, V. J. S., et al. 2001, ApJ, 556, 830
Bertout, C., Robichon, N., & Arenou, F. 1999, A&A, 352, 574
Bonnell, I. A., Bate, M. R., & Vine, S. G. 2003, MNRAS, 343, 413
Boss, A. 1988, ApJ, 331, 370
———. 2001, ApJ, 551, L167
Boulanger, F., Bronfman, L., Dame, T. M., & Thaddeus, P. 1998, A&A, 332, 273
Brandner, W., & Zinnecker, H. 1997, A&A, 321, 220
Briceño, C., Hartmann, L., Stauffer, J. R., Gagne, M., Stern, R. A., & Caillault, J.-P. 1997, AJ, 113, 740
Briceño, C., Luhman, K. L., Hartmann, L., Stauffer, J. R., & Kirkpatrick, J. D. 2002, ApJ, 580, 317
Burrows, A., et al. 1997, ApJ, 491, 856
Cambrésy, L., et al. 1997, A&A, 324, L5
Carpenter, J. M., Hillenbrand, L. A., Skrutskie, M. F., & Meyer, M. R. 2002, AJ, 124, 1001
Chabrier, G., Baraffe, I., Allard, F., & Hauschildt, P. 2000, ApJ, 542, L119
Chelli, A., Cruz-Gonzalez, I., & Reipurth, B. 1995, A&AS, 114, 135
Comerón, F., Neuhäuser, R., & Kaas, A. A. 2000, A&A, 359, 269
Comerón, F., Reipurth, B., Henry, A., & Fernández, M. 2004, A&A, 417, 583
Comerón, F., Rieke, G. H., & Neuhäuser, R. 1999, A&A, 343, 477
Correia, S., Zinnecker, H., Ratzka, Th., & Sterzik, M. F. 2006, A&A, 459, 909
Covino, E., Alcala, J. M., Allain, S., Bouvier, J., Terranegra, L., & Krautter, J. 1997, A&A, 328, 187
Cruz, K. L., et al. 2007, AJ, 133, 439
Dahn, C. C., et al. 2002, AJ, 124, 1170
Delgado-Donate, E. J., Clarke, C. J., & Bate, M. R. 2003, MNRAS, 342, 926
Dobbie, P. D., Kenyon, F., Jameson, R. F., & Hodgkin, S. T. 2002, MNRAS, 331, 445
Elmegreen, B. G. 2000, ApJ, 530, 277
Epchtein, N., et al. 1999, A&A, 349, 236
Feigelson, E. D. 1996, ApJ, 468, 306
Feigelson, E. D., & Kriss, G. A. 1989, ApJ, 338, 262
Feigelson, E. D., & Lawson, W. A. 2004, ApJ, 614, 267
Feigelson, E. D., Lawson, W. A., & Garmire, G. P. 2003, ApJ, 599, 1207
Filippenko, A. V. 1982, PASP, 94, 715
Gauvin, L. S., & Strom, K. M. 1992, ApJ, 385, 217
Ghez, A. M., McCarthy, D. W., Patience, J. L., & Beck, T. L. 1997, ApJ, 481, 378
Gómez, M., & Mardones, D. 2003, AJ, 125, 2134
Goodwin, S. P., & Whitworth, A. 2007, A&A, 466, 943
Haisch, K. E., Greene, T. P., Barsony, M., & Stahler, S. W. 2004, AJ, 127, 1747
Hartigan, P. 1993, AJ, 105, 1511
Hartmann, L. 1998, Accretion Processes in Star Formation (Cambridge: Cambridge Univ. Press)
———. 2001, AJ, 121, 1030
———. 2002, ApJ, 578, 914
Hartmann, L., Ballesteros-Paredes, J., & Bergin, E. 2001, ApJ, 562, 852
Hillenbrand, L. A. 1997, AJ, 113, 1733
Hillenbrand, L. A., & Carpenter, J. M. 2000, ApJ, 540, 236
Hillenbrand, L. A., & Hartmann, L. W. 1998, ApJ, 492, 540
Huenemoerder, D. P., Lawson, W. A., & Feigelson, E. D. 1994, MNRAS, 271, 967
Kenyon, S. J., & Hartmann, L. 1995, ApJS, 101, 117
Kirkpatrick, J. D., et al. 2006, ApJ, 639, 1120
Kraus, A. L., & Hillenbrand, L. A. 2007, ApJ, 662, 413
Kroupa, P., & Bouvier, J. 2003, MNRAS, 346, 369
Landolt, A. U. 1992, AJ, 104, 340
Larson, R. B. 1985, MNRAS, 214, 379
———. 1995, MNRAS, 272, 213
Leggett, S. K. 1992, ApJS, 82, 351
Levine, J. L., Steinhauer, A., Elston, R. J., & Lada, E. A. 2006, ApJ, 646, 1215
López Martí, B., Eislöffel, J., Scholz, A., & Mundt, R. 2004, A&A, 416, 555
Low, C., & Lynden-Bell, D. 1976, MNRAS, 176, 367
Lucas, P. W., Roche, P. F., Allard, F., & Hauschildt, P. H. 2001, MNRAS, 326, 695
Lucas, P. W., Roche, P. F., & Tamura, M. 2005, MNRAS, 361, 211
Lucas, P. W., Weights, D. J., Roche, P. F., & Riddick, F. C. 2006, MNRAS, 373, L60

Luhman, K. L. 1999, ApJ, 525, 466
———. 2000, ApJ, 544, 1044
———. 2001, ApJ, 560, 287
———. 2004a, ApJ, 602, 816
———. 2004b, ApJ, 614, 398
———. 2004c, ApJ, 616, 1033
———. 2004d, ApJ, 617, 1216
———. 2006, ApJ, 645, 676
———. 2007, in ASP Conf Ser., Handbook of Star Forming Regions, ed. B. Reipurth (San Francisco: ASP), submitted
Luhman, K. L., Briceño, C., Stauffer, J. R., Hartmann, L., Barrado y Navascués, D., & Caldwell, N. 2003a, ApJ, 590, 348
Luhman, K. L., Peterson, D. E., & Megeath, S. T. 2004, ApJ, 617, 565
Luhman, K. L., & Potter, D. 2006, ApJ, 638, 887
Luhman, K. L., Stauffer, J. R., & Mamajek, E. E. 2005a, ApJ, 628, L69
Luhman, K. L., et al. 2000, ApJ, 540, 1016
———. 2003b, ApJ, 593, 1093
———. 2005b, ApJ, 631, L69
———. 2005c, ApJ, 635, L93
———. 2006, ApJ, 649, 894
Meyer, M. R., Adams, F. C., & Larson, R. B. 2000, in Protostars & Planets IV, ed. V. Mannings, A. P. Boss, & S. S. Russell (Tucson: Univ. Arizona Press), 121
Mizuno, A., et al. 2001, PASJ, 53, 1071
Muench, A. A., Lada, E. A., Lada, C. J., & Alves, J. 2002, ApJ, 573, 366
Muench, A. A., et al. 2003, AJ, 125, 2029
Muzerolle, J., Luhman, K. L., Briceño, C., Hartmann, L., & Calvet, N. 2005, ApJ, 625, 906
Neuhäuser, R., & Comerón, F. 1999, A&A, 350, 612
Padoan, P., & Nordlund, Å. 2002, ApJ, 576, 870
Palla, F., & Galli, D. 1997, ApJ, 476, L35
Palla, F., & Stahler, S. W. 1999, ApJ, 525, 772
———. 2000, ApJ, 540, 255
Palla, F., & Stahler, S. W. 2002, ApJ, 581, 1194
Perryman, M. A. C., et al. 1997, A&A, 323, L49
Persi, P., Tapia, M., Gómez, M., Roth, M., & Marenzi, A. R. 2005, A&A, 431, 539
Persi, P., et al. 2000, A&A, 357, 219
Preibisch, T., Stanke, T., & Zinnecker, H. 2003, A&A, 409, 147
Rees, M. J. 1976, MNRAS, 176, 483
Reid, I. N., & Gizis, J. E. 1997, AJ, 113, 2246
Reipurth, B., & Clarke, C. 2001, AJ, 122, 432
Reipurth, B., Nyman, L.-Å., & Chini, R. 1996, A&A, 314, 258
Reipurth, B., & Zinnecker, H. 1993, A&A, 278, 81
Rydgren, A. E. 1980, AJ, 85, 444
Saffe, C., Randich, S., Mardones, D., Caselli, P., Persi, P., & Racca, G. 2003, A&A, 409, 993
Silk, J. 1977, ApJ, 214, 152
Sirianni, M., et al. 2005, PASP, 117, 1049
Skrutskie, M., et al. 2006, AJ, 131, 1163
Slesnick, C. L., Carpenter, J. M., Hillenbrand, L. A., & Mamajek, E. E. 2006, AJ, 132, 2665
Slesnick, C. L., Hillenbrand, L. A., & Carpenter, J. M. 2004, ApJ, 610, 1045
Steele, I. A., & Howells, L. 2000, MNRAS, 313, L43
Stelzer, B., Micela, G., & Neuhäuser, R. 2004, A&A, 423, 1029
Telleschi, A., Güdel, M., Briggs, K. R., Audard, M., & Palla, F. 2007, A&A, 468, 425
Umbreit, S., Burkert, A., Henning, T., Mikkola, S., & Spurzem, R. 2005, ApJ, 623, 940
Whittet, D. C. B., Kirrane, T. M., Kilkenny, D., Oates, A. P., Watson, F. G., & King, D. J. 1987, MNRAS, 224, 497
Whittet, D. C. B., et al. 1997, A&A, 327, 1194
Whitworth, A. P., & Stamatellos, D. 2006, A&A, 458, 817
Wichmann, R., Bastian, U., Krautter, J., Jankovics, I., & Ruciński, S. M. 1998, MNRAS, 301, L39